Mon. Not. R. Astron. Soc. **000**, 1–26 (2013) Printed 9 November 2016 (MN LATEX style file v1.4)

# Dissecting the Evolution of Dark Matter Subhaloes in the Bolshoi Simulation

Frank C. van den Bosch⋆
*Department of Astronomy, Yale University, PO. Box 208101, New Haven, CT 06520-8101*

arXiv:1611.02657v1 [astro-ph.GA] 8 Nov 2016

**ABSTRACT**
We present a comprehensive analysis of the evolution of dark matter subhaloes in the cosmological Bolshoi simulation. We identify a complete set of 12 unique evolution channels by which subhaloes evolve in between simulation outputs, and study their relative importance and demographics. We show that instantaneous masses and maximum circular velocities of individual subhaloes are extremely noisy, despite the use of a sophisticated, phase-space-based halo finder. We also show that subhaloes experience frequent penetrating encounters with other subhaloes (on average about one per dynamical time), and that subhaloes whose apo-center lies outside the virial radius of their host (the 'ejected or 'backsplash haloes) experience tidal forces that modify their orbits. This results in an average fractional subhalo exchange rate among host haloes of $\sim 0.01$ Gyr$^{-1}$ (at the present time). In addition, we show that there are three distinct disruption channels; one in which subhaloes drop below the mass resolution limit of the simulation, one in which subhaloes 'merge' with their host halo largely driven by dynamical friction, and one in which subhaloes abruptly disintegrate. We estimate that roughly 80 percent of all subhalo disruption in the Bolshoi simulation is numerical, rather than physical. This 'over-merging is a serious road-block for the use of numerical simulations to interpret small scale clustering, or for any other study that is sensitive to the detailed demographics of dark matter substructure.

**Key words:** methods: analytical — methods: statistical — galaxies: formation — galaxies: haloes — galaxies: kinematics and dynamics — cosmology: dark matter

## 1 INTRODUCTION

During the hierarchical assembly of dark matter haloes, the inner regions of early virialized objects often survive accretion on to a larger system, thus giving rise to a population of subhaloes. Dark matter substructure plays an important role in many areas of astrophysics. It causes time-delays (e.g. Keeton & Moustakas 2009) and flux-ratio anomalies (Metcalf & Madau 2001; Bradač et al. 2002; Dalal & Kochanek 2002) in gravitational lensing, it boosts the dark matter annihilation signal from dark matter haloes (e.g. Diemand, Kuhlen & Madau 2007; Giocoli, Pieri & Tormen 2008; Pieri, Bertone & Branchini 2008), and impacts the dynamics of tidal streams and galactic discs (e.g., Tóth & Ostriker 1992; Taylor & Babul 2001; Ibata et al. 2002; Carlberg 2009). In addition, dark matter subhaloes host satellite galaxies and the demographics of dark matter substructure is therefore directly related to the (small scale) clustering of galaxies. This latter idea underlies the popular technique of subhalo abundance matching (e.g., Vale & Ostriker 2004; Conroy, Wechsler & Kravtsov 2006, 2007; Guo et al. 2010; Hearin et al. 2013), which has become a prime tool for interpreting galaxy clustering, galaxy-galaxy lensing, group multiplicity functions, and for constraining cosmological parameters (e.g., Conroy et al. 2006; Marin et al. 2008; Trujillo-Gomez et al. 2011; Hearin et al. 2013, 2014, 2016; Reddick et al. 2013, 2014; Zentner et al. 2014, 2016; Lehmann et al. 2015).

Dark matter subhaloes are subjected to forces that try to dissolve it: dynamical friction, tides from the host halo, and impulsive encounters with other substructure. Because of the complex interplay of these numerous, non-linear processes the formation and evolution of dark matter substructure is best studied using numerical $N$-body simulations. Nowadays, large cosmological simulations routinely resolve an entire hierarchy of substructure, with haloes hosting subhaloes, which themselves host sub-subhaloes, etc. These simulations are used as the bedrock for semi-analytical models of galaxy formation (e.g., Kauffmann, Nusser & Steinmetz 1997; Croton et al. 2006; De Lucia & Blaizot 2007; Kang & van den Bosch 2008; Fontanot et al. 2012), to interpret large scale structure data with the help of halo occupation models (e.g., Conroy et al. 2006; Marín et al. 2008; Zentner

⋆ E-mail: frank.vandenbosch@yale.edu

© 2013 RAS

et al. 2016), to study the impact of substructure on gravitational lensing (e.g., Bradač et al. 2004; Amara et al. 2006; Maccío et al. 2006; Xu et al. 2015), and even to constrain cosmological parameters (e.g., Reddick et al. 2014).

All these methods are ultimately limited by the accuracy of the numerical simulations used. It wasn't until the end of the 1990's that numerical simulations started to reach sufficient mass and force resolution to resolve a surviving population of subhaloes (Moore, Katz & Lake 1996; Tormen, Bouchet & White 1997; Brainerd, Goldberg & Villumsen 1998; Moore et al. 1998; Ghigna et al. 1998; Tormen, Diaferio & Syer 1998; Klypin et al. 1999). And even today, the limiting mass and force resolution of numerical simulations implies an over-merging of substructure, especially near the centers of their host haloes. In addition, the actual detection and characterization of substructure in simulations is another important source of error. Different subhalo finders can yield very different results, even when applied to the same simulation (e.g., van den Bosch & Jiang 2016). Hence, it is prudent that we continue to scrutinize the numerical simulations that we use to interpret our ever increasing amount of astrophysical data.

In this paper we examine the evolution of dark matter substructure in a pure dark matter-only simulation. We identify a complete set of 12 unique evolution channels, by which subhaloes evolve in between different simulation outputs, and we study the frequencies and demographics of these evolution channels in detail. We show that instantaneous masses and maximum circular velocities of individual subhaloes are extremely noisy, even when these have been obtained using sophisticated, phase-space-based subhalo finders. We also show that subhaloes experience frequent penetrating encounters with other subhaloes (on average about one per dynamical time), and that most subhaloes that are on orbits that take them outside of their host (the so-called ejected or backsplash haloes) experience tidal forces that modify their orbital parameters. In addition, we show that there are three distinct disruption channels; one in which subhaloes drop below the mass resolution limit of the simulation, one in which subhaloes 'merge' with their host halo largely driven by dynamical friction, and one in which subhaloes seem to spontaneously disintegrate.

This paper is organized as follows. Section 2 describes the numerical simulations and merger trees used in this study. In §3 and §4 we introduce a complete set of 12 unique subhalo evolution channels, discuss their demographics and relative importance for describing the evolution of subhaloes in the Bolshoi simulation. Section 5 takes a closer look at the tidal evolution of dark matter subhaloes, focusing on tidal stripping, penetrating encounters among subhaloes, and subhalo disruption. We summarize our findings in §6.

## 2 METHODOLOGY

### 2.1 Numerical Simulation

To study the evolution of dark matter substructure, we use the large 'Bolshoi' simulation (Klypin et al. 2011), which follows the evolution of $2048^3$ dark matter particles using the Adaptive Refinement Tree (ART) code (Kravtsov, Klypin & Khokhlov 1997) in a flat ΛCDM model with parameters $\Omega_{\rm m,0} = 1 - \Omega_{\Lambda,0} = 0.27$, $\Omega_{\rm b,0} = 0.0469$, $h = H_0/(100\,{\rm km\,s^{-1}\,Mpc^{-1}}) = 0.7$, $\sigma_8 = 0.82$ and $n_{\rm s} = 0.95$ (hereafter 'Bolshoi cosmology'). The box size of the Bolshoi simulation is $L_{\rm box} = 250h^{-1}$ Mpc, resulting in a particle mass of $m_{\rm p} = 1.35 \times 10^8\, h^{-1}{\rm M}_\odot$.

We use the publicly available halo catalogs[†] obtained using the phase-space halo finder ROCKSTAR (Behroozi et al. 2013a), which uses adaptive, hierarchical refinement of friends-of-friends groups in six phase-space dimensions and one time dimension. As demonstrated in Knebe et al. (2011, 2013), this results in a very robust identification of (sub)haloes (see also van den Bosch & Jiang 2016). ROCKSTAR haloes are defined as spheres with an average density equal to $\Delta_{\rm vir}(z)\rho_{\rm crit}(z)$. Here $\rho_{\rm crit}(z) = 3H^2(z)/8\pi G$ is the critical density for closure at redshift $z$, and $\Delta_{\rm vir}(z)$ is given by the fitting function of Bryan & Norman (1998).

We use the 19 simulation outputs at $z \leq 0.0605$, which are output every $\Delta a = 0.003$ ($a$ is the scale factor), corresponding to roughly $\Delta t = 42$ Myr. Throughout we split the halo population in three categories:

- host haloes; these are distinct haloes that are not, and never have been, located within the virial radius of another, more massive halo.
- subhaloes; these are haloes that are located within the virial radius of another, more massive halo.
- ejected haloes; these are distinct haloes whose main progenitor has at one or more occasions passed through the virial region of a more massive halo. Ejected haloes are also sometimes called 'backsplash' haloes.

As shown in van den Bosch et al. (2014), host haloes clearly dominate, with a fraction that increases from $\sim 70$ percent for haloes with $M_{\rm h} = 10^{11}\,h^{-1}{\rm M}_\odot$ to 100 percent at the massive end. The remainder is split roughly equally between subhaloes and ejected haloes. Following Jiang & van den Bosch (2016a), we also distinguish between subhaloes of different order: we refer to subhaloes as first-order subhaloes, to sub-subhaloes (i.e., subhaloes located within the virial radius of another subhalo) as second-order subhaloes, etc. An $n^{\rm th}$-order (sub)halo that hosts an $(n+1)^{\rm th}$-order subhalo is called a *parent* halo of the $(n+1)^{\rm th}$-order subhalo. Note that the masses of (sub)haloes are defined such that the mass of an $n^{\rm th}$-order parent halo *includes* the masses of its subhaloes of order $n+1$.

Throughout this paper we restrict ourselves to first-order subhaloes with mass $m \geq m_{50} \equiv 10^{9.83}\ h^{-1}{\rm M}_\odot$ (corresponding to $\geq 50$ particles per halo) that reside in host haloes with mass in the range $10^{11.5}\ h^{-1}{\rm M}_\odot \leq {\rm M_h} \leq 10^{15}\ {\rm h^{-1}M}_\odot$, and we discard any subhalo whose orbital energy is positive, indicating that the subhalo is not bound to its host halo (see §4 for details on how the orbital energy is calculated). The reason for only considering subhaloes with at least 50 particles is that below this mass limit the subhalo mass functions are starting to become incomplete due to limiting mass and/or force resolution (see van den Bosch & Jiang 2016).

[†] http://hipacc.ucsc.edu/Bolshoi/MergerTrees.html

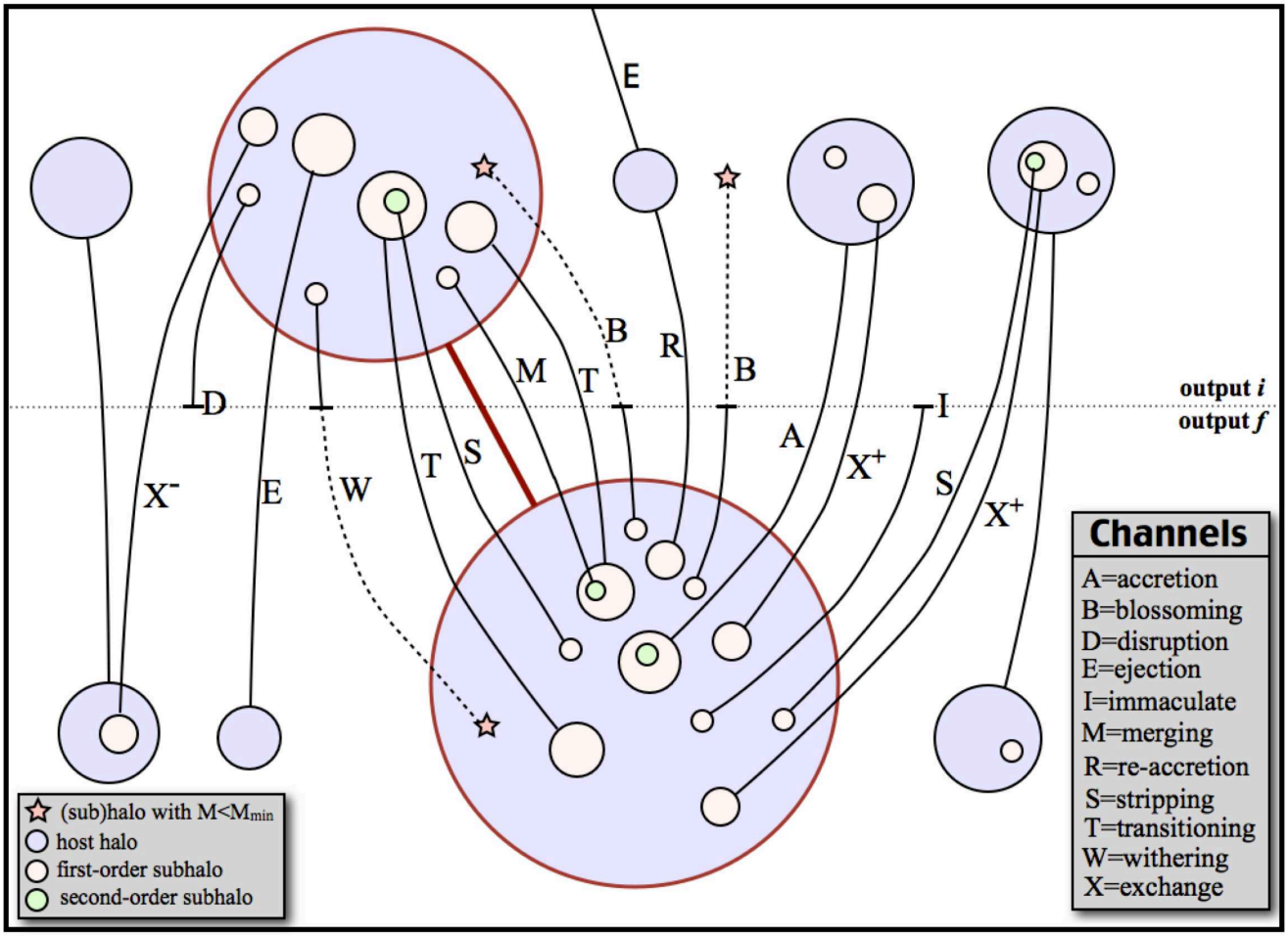


**Figure 1.** Illustration of the various subhalo evolution channels (SECs). The large circles with red rims, linked by a thick red line, indicate host haloes in $\mathcal{S}_{\rm i}$ (upper) and $\mathcal{S}_{\rm f}$. All other sets of circles linked together correspond to a particular SEC, as labeled. Detailed descriptions of the various channels can be found in §3 and in Table 1.

### 2.2 Merger Trees

The halo catalogs at different simulation outputs, constructed using the `ROCKSTAR` halo finder, are linked across outputs using the `Consistent` merger tree algorithm of Behroozi et al. (2013b). We refer the interested reader to that paper for details, but here highlight a few aspects that are of particular relevance to this paper.

The first step of constructing the merger trees is assigning each halo at time step $t_n$ a descendant halo at the later time step $t_{n+1}$. This is done by identifying the halo at $t_{n+1}$ that receives the largest fraction of the particles (excluding substructure) of the halo in question at $t_n$. Next, the resulting links are improved upon by using orbit integration to predict the positions and velocities of (sub)haloes detected across adjacent outputs. In particular, particle-based links between halos that are too far apart in position, velocity or mass are cut and reconnected to more likely candidates.

Some (sub)haloes identified at time step $t_{n+1}$ may end up having no progenitor halo at $t_n$. This may indicate that the progenitor halo has a mass below the mass-completeness limit of the simulation, or that the progenitor halo is missing from the halo catalog at time step $t_n$. To account for the latter case, the merger tree algorithm creates a placeholder halo, called a *phantom halo*, in the halo catalog corresponding to $t_n$, with a mass, position and velocity computed based on those at $t_{n+1}$ (see Behroozi et al. 2013b for details). Phantom haloes may be created for up to four successive time steps to allow for cases in which the halo finder looses track of a (sub)halo for multiple time steps. They therefore 'repair' failures of the halo finder by patching and interpolating across multiple outputs. If a (sub)halo at $t_{n+1}$ has no progenitors in any of the four previous time steps, it is assumed that the halo formed at $t_{n+1}$, and the corresponding place-holder haloes in the previous four time steps are removed from the catalogs.

If a (sub)halo at output $t_n$ has no descendant at $t_{n+1}$, or is not the most massive progenitor of its descendant, either the halo is a spurious 'fluctuation', or it was completely disrupted during the time interval between the two time steps (Behroozi et al. 2013b refer to the latter as a 'tidal merger'). In order to discriminate between these two options, only

**Table 1.** Subhalo Evolution Channels

| (1) | (2) | (3) | (4) |
|---|---|---|---|
| T | Transition | fwd | subhaloes in $\mathcal{S}_{\rm i}$ that end up as subhaloes in $\mathcal{S}_{\rm f}$ |
| A | Accretion | bwd | subhaloes in $\mathcal{S}_{\rm f}$ that were host haloes at time $t_{\rm i}$ |
| R | Re-accretion | bwd | subhaloes in $\mathcal{S}_{\rm f}$ that were ejected haloes at time $t_{\rm i}$ |
| E | Ejection | fwd | subhaloes in $\mathcal{S}_{\rm i}$ that are host haloes at $t_{\rm f}$ |
| D | Disruption | fwd | subhaloes in $\mathcal{S}_{\rm i}$ that are disrupted at $t_{\rm f}$ |
| S | Stripping | bwd | subhaloes in $\mathcal{S}_{\rm i}$ that were subhaloes of order $n \geq 2$ at $t_{\rm i}$ |
| M | Merging | fwd | subhaloes in $\mathcal{S}_{\rm i}$ that end up as subhaloes of order $n \geq 2$ at $t_{\rm f}$ |
| W | Withering | fwd | subhaloes in $\mathcal{S}_{\rm i}$ that end up as subhaloes with $m < m_{50}$ at $t_{\rm f}$ |
| B | Blossoming | bwd | subhaloes in $\mathcal{S}_{\rm f}$ whose progenitor has a mass $m < m_{50}$ at $t_{\rm i}$ |
| I | Immaculate | bwd | subhaloes in $\mathcal{S}_{\rm f}$ without progenitor at $t_{\rm i}$ |
| $X^+$ | eXchange | bwd | subhaloes in $\mathcal{S}_{\rm f}$ that were subhaloes at $t_{\rm i}$ but not in the main progenitor of their current host |
| $X^-$ | eXchange | fwd | subhaloes in $\mathcal{S}_{\rm i}$ that end up as subhaloes at $t_{\rm f}$ but not in the descendent of their current host |

Definition of the various SEC channels that describe the evolution of subhaloes in set $\mathcal{S}_{\rm i}$ at time $t_{\rm i}$ to that of subhaloes in set $\mathcal{S}_{\rm f}$ at a later time $t_{\rm f}$. Here $\mathcal{S}_{\rm i}$ and $\mathcal{S}_{\rm f}$ are linked by the fact that the host haloes of $\mathcal{H}_{\rm i}$ are the main progenitors of the host haloes of $\mathcal{H}_{\rm f}$. Column (1) indicates the letter symbol we use throughout, column (2) lists the name of the SEC, column (3) indicates whether it is a forward (fwd) or backward (bwd) channel, and column (4) gives a concise description.

those haloes that at time step $t_n$ experience a tidal acceleration $|\mathcal{T}| \geq GM(r)/r^3 > 0.4\,{\rm km\,s^{-1}\,Myr^{-1}}$ comoving ${\rm Mpc}^{-1}$ are considered as 'true' haloes that are disrupted. A halo that does not exceed this tidal limit is considered a 'merger fluctuation' and is removed from the halo catalog, *together with all its progenitors at all previous timesteps*. We emphasize that these merger fluctuations are not necessarily haloes close to the mass-completeness limit of the simulation. For example, around $z \sim 0$ roughly $3 \times 10^{-4}$ of haloes with mass $\sim 10^{12}\,h^{-1}{\rm M}_\odot$ are identified as merger fluctuations (P. Behroozi, priv. communication).

## 3 SUBHALO EVOLUTION CHANNELS

Consider two simulation outputs, conveniently labeled $i$ (for initial) and $f$ (for final), with corresponding redshifts $z_{\rm f} < z_{\rm i}$. We start by identifying all host haloes in output $f$ in a given mass range. We denote this set by $\mathcal{H}_{\rm f}$. Next we identify the set $\mathcal{S}_{\rm f}$ of all *first-order* subhaloes with mass $m \geq m_{50}$ belonging to host haloes in $\mathcal{H}_{\rm f}$. Subsequently we move to output $i$, and first identify the set $\mathcal{H}_{\rm i}$ of the main progenitors of $\mathcal{H}_{\rm f}$. Finally, we identify the set $\mathcal{S}_{\rm i}$ of all *first-order* subhaloes with $m \geq m_{50}$ belonging to host haloes in $\mathcal{H}_{\rm i}$. In what follows, we use $\mathcal{S}$ to denote the union of $\mathcal{S}_{\rm i}$ and $\mathcal{S}_{\rm f}$ (i.e., $\mathcal{S} = \mathcal{S}_{\rm i} \cup \mathcal{S}_{\rm f}$). Similarly, $\mathcal{H} = \mathcal{H}_{\rm i} \cup \mathcal{H}_{\rm f}$.

The goal of this paper is to study what happens between redshifts $z_{\rm i}$ and $z_{\rm f}$ to the subhaloes in $\mathcal{S}_{\rm i}$ (we call this the 'forward evolution channels'), and how the subhaloes in $\mathcal{S}_{\rm f}$ end up in their host haloes (we call this the 'backward evolution channels'). By carefully studying the subhaloes in $\mathcal{S}$, as well as their progenitors and/or descendants, we have identified a total of 12 subhalo evolution channels (hereafter SECs); 6 forward channels and 6 backward channels (see Fig. 1 for an illustration). This set is both complete and unique, in that each and every subhalo in $\mathcal{S}$ is associated with one, and only one, channel. In order of diminishing importance, these are:

- The Transition channel T: these are subhaloes in $\mathcal{S}_{\rm i}$ that end up as subhaloes in $\mathcal{S}_{\rm f}$. As we will see, this is the most common evolution channel, by far. Although we refer to the transition channel as a forward channel, it is equally valid to consider it a backward channel.
- The Accretion channel A: these are subhaloes in $\mathcal{S}_{\rm f}$ that were host haloes at time $t_{\rm i}$. Hence, they were accreted, for the first time in their existence, into a host halo in the time interval between $t_{\rm i}$ and $t_{\rm f}$.
- the Ejection channel E: these are subhaloes in $\mathcal{S}_{\rm i}$ that are host haloes at $t_{\rm f}$. This channel is the inverse of the accretion channel. Note that ejection does not imply that the subhalo is no longer bound to its host halo; it merely implies that its center is no longer located within the host halo's virial extent.
- the Re-accretion channel R: these are subhaloes in $\mathcal{S}_{\rm f}$ that were ejected haloes at time $t_{\rm i}$. Note that they do not necessarily have to have been ejected from the same host halo into which they are now being re-accreted.
- the Stripping channel S: these are (first-order) subhaloes in $\mathcal{S}_{\rm f}$ that were subhaloes of order $n \geq 2$ at $t_{\rm i}$. Recall that a subhalo is said to be of order $n$ if it is located within the extent of another subhalo of order $n-1$.
- the Merging channel M: these are (first-order) subhaloes in $\mathcal{S}_{\rm i}$ that end up as subhaloes of order $n \geq 2$ at $t_{\rm f}$. This channel is the inverse of the stripping channel.
- the Withering channel W: these are subhaloes in $\mathcal{S}_{\rm i}$ that end up as subhaloes with $m < m_{50}$ at $t_{\rm f}$. Hence, they are similar to T-subhaloes, except that mass loss causes them to drop out of our mass-limited sample.
- the Blossoming channel B: these are subhaloes in $\mathcal{S}_{\rm f}$ whose progenitor has a mass $m < m_{50}$ at $t_{\rm i}$. This channel is the inverse of the withering channel, and refers to subhaloes that have increased their mass between $t_{\rm i}$ and $t_{\rm f}$ from below to above the mass limit of our sample.
- the Disruption channel D: these are subhaloes in $\mathcal{S}_{\rm i}$ that are disrupted at $t_{\rm f}$. Note that this is different from the withering channel, in that W subhaloes *do* have a descendant in the halo catalogue, but with a mass below the sample limit. D subhaloes are identified in the `ROCKSTAR` halo catalog at $t_{\rm i}$ as having `mmp`$= 0$.
- the Immaculate channel I: these are subhaloes in $\mathcal{S}_{\rm f}$ without progenitor at $t_{\rm i}$. This channel is the inverse of the

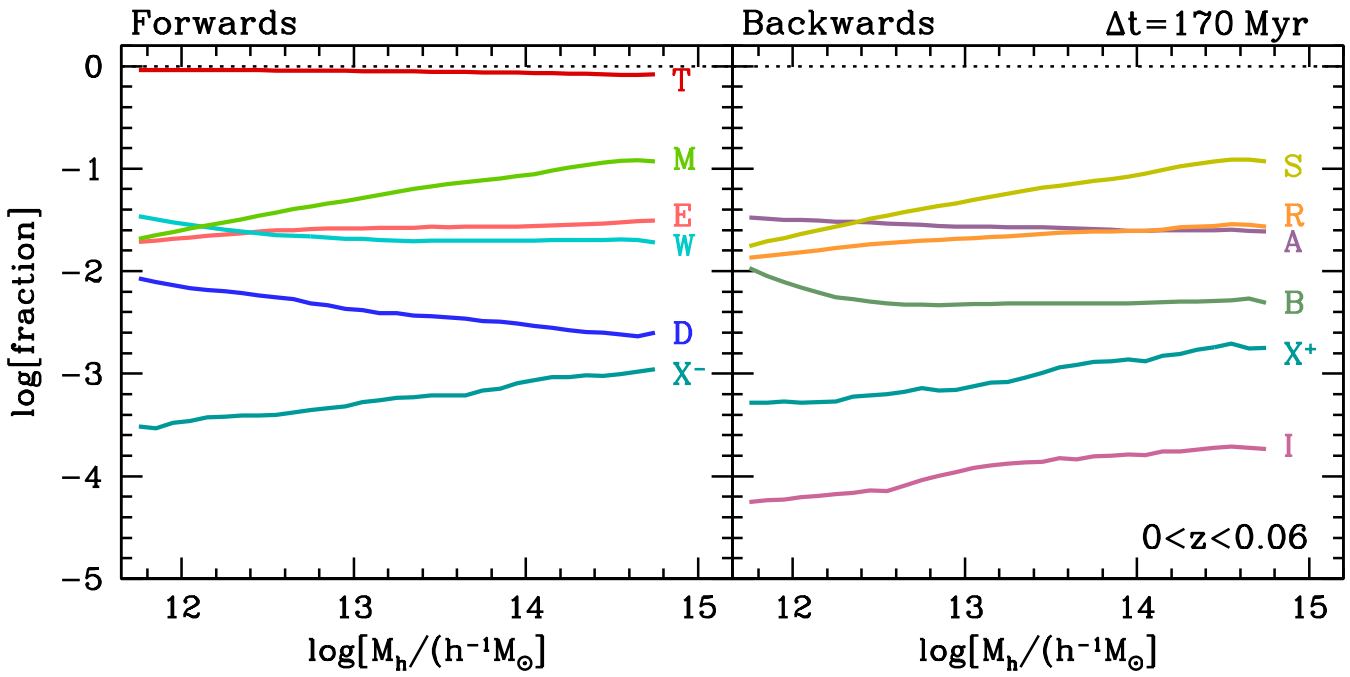


**Figure 2.** The fractions of subhaloes that evolve in a time step of $\Delta t = 170\,\mathrm{Myr}$ along different SECs. Results are shown as function of halo mass and averaged over all simulation outputs with $z < 0.06$. See Fig. 1 and Table 1 for an illustration and description of the various SECs.

disruption channel, and identifies subhaloes that appear in the ROCKSTAR halo catalog at $t_\mathrm{f}$ as a subhalo without having an (identified) progenitor at $t_\mathrm{i}$. I subhaloes are identified in the halo catalog at $t_\mathrm{f}$ as having $\mathtt{num}_\mathrm{prog} < 1$ and PID$> 0$.

- the positive eXchange channel $\mathrm{X}^+$: these are subhaloes in $\mathcal{S}_\mathrm{f}$ that were subhaloes at $t_\mathrm{i}$ but not in the main progenitor of their current (at $t_\mathrm{f}$) host halo.
- the negative eXchange channel $\mathrm{X}^-$: these are subhaloes in $\mathcal{S}_\mathrm{i}$ that end up as subhaloes at $t_\mathrm{f}$ but not in the descendent of their current (at $t_\mathrm{i}$) host halo. This channel is the inverse of the $\mathrm{X}^+$ channel.

A list of concise descriptions for each SEC can be found in Table 1. In what follows we will refer to each channel with the capital letter indicated above and in the first column of Table 1. Finally, it is important to be aware of the following: Ejection and re-accretion can go unnoticed if both happen within the time-interval between the two simulation outputs. In that case the subhalo is assigned to the transition channel, T. In addition, if a subhalo is ejected and subsequently captured by another host halo, the subhalo is assigned to the negative exchange channel, $\mathrm{X}^-$, rather than the ejection channel.

### 3.1 The Relative Importance of different SECs

Given two simulation outputs, at $t_\mathrm{i}$ and $t_\mathrm{f}$, a range in host halo mass, and the corresponding sets of subhaloes, $\mathcal{S}_\mathrm{i}$ and $\mathcal{S}_\mathrm{f}$, we determine for each subhalo in $\mathcal{S}$ to which of the twelve SEC channels it belongs. Next we compute the fractional contributions (by number) for each of these channels, which are defined as

$$f_\mathrm{c} \equiv \begin{cases} N_\mathrm{c}/N_\mathrm{i} & \text{if forward channel} \\ N_\mathrm{c}/N_\mathrm{f} & \text{if backward channel} \end{cases} \qquad (1)$$

Here $N_\mathrm{c}$ is the number of subhaloes belonging to channel 'c' and $N_\mathrm{i}$ and $N_\mathrm{f}$ are the total number of subhaloes in $\mathcal{S}_\mathrm{i}$ and $\mathcal{S}_\mathrm{f}$, respectively.

Fig. 2 plots $f_\mathrm{c}$ for the various forward (left-hand panel) and backward (right-hand panel) channels as function of the mass of the host halo at the later output (i.e., at $t_\mathrm{f}$). These fractions correspond to a time interval in between simulation outputs of $\Delta t = 170\,\mathrm{Myr}$. Among the 19 simulation outputs used here, there are a total of 14 pairs that are (roughly) separated by this time-interval, and the fractions shown are the averages among those 14 pairs. Note that the time intervals between $t_\mathrm{i}$ and $t_\mathrm{f}$ considered throughout this paper are sufficiently short that the host halo masses evolve very little. For instance, for $\Delta t = 170\,\mathrm{Myr}$ the average host halo in our sample only increases its mass by 0.9 percent.

By far the dominant channel is the transition channel T, which describes subhaloes that simply continue to orbit within one and the same host halo. Next up in order of importance, are the stripping, S, and merging, M, channels. These describe subhaloes that either decrease or increase their order between $t_\mathrm{i}$ and $t_\mathrm{f}$, respectively. Both contribute more in more massive host haloes, reaching fractional contributions of $\sim 10$ percent in cluster-size hosts. The fractional contribution of accretion of new subhaloes, A, is similar to that of ejection, E, and re-accretion, R, which as we will see in §4.2 is in agreement with simple expectations based on the orbits of subhaloes at infall.

Another channel that contributes roughly equally is the withering channel, W, which describes subhaloes that experience mass loss between $t_\mathrm{i}$ and $t_\mathrm{f}$ such that at $t_\mathrm{f}$ their mass has dropped below the limit of 50 particles per halo. The inverse of the withering channel is the blossoming channel, B, which describes subhaloes whose mass has increased from below $m_{50}$ to above $m_{50}$ in the time interval between

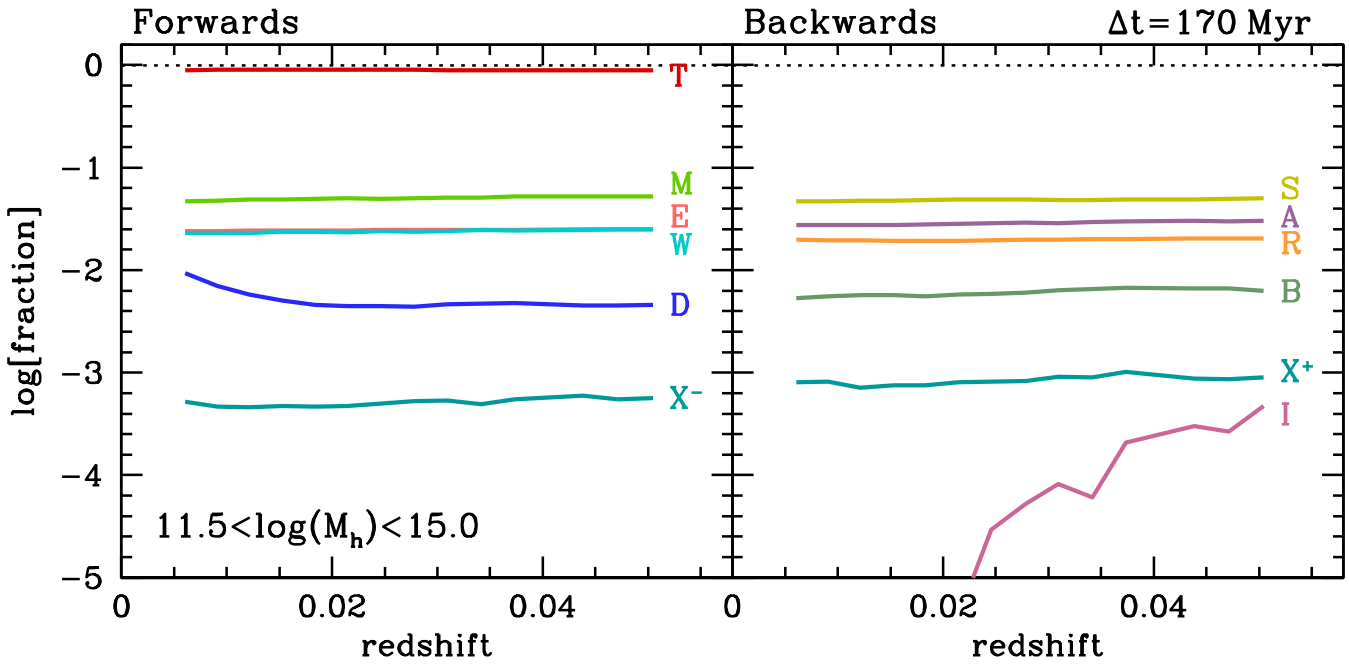


**Figure 3.** Same as Fig. 2, but this time the fractions are computed for host haloes in the range $10^{11.5} \leq M_{\rm h} \leq 10^{14.5}\,h^{-1}{\rm M}_\odot$ and plotted as a function of the average redshift between the two epochs separated by $\Delta t = 170\,{\rm Myr}$.

$t_{\rm i}$ and $t_{\rm f}$. Blossoming subhaloes contribute between $\sim 1\%$ in low mass host haloes and $\sim 0.5\%$ at the massive end, and as we will see, are mainly a 'by-product' of noise in the subhalo mass assignment (see §4.4). Channel D describes subhaloes that disrupt between $t_{\rm i}$ and $t_{\rm f}$, and contributes between one percent ($M_{\rm h} \sim 10^{12}\,h^{-1}{\rm M}_\odot$) and 0.3 percent ($M_{\rm h} \sim 10^{15}\,h^{-1}{\rm M}_\odot$).

The positive and negative exchange channels, $\rm X^+$ and $\rm X^-$, respectively, typically contribute only $\lesssim 0.1\%$, with a weak dependence on host halo mass. Exchange channels basically describe 'ejection' followed by 're-accretion', except that the subhalo is re-accreted into another host halo than the one from which it was ejected. As is evident from Fig. 1, another contribution to the $\rm X^+$ channel is from a combination of accretion plus stripping. If both processes occur within the same time-interval, this subhalo will be assigned to the $\rm X^+$ channel. Finally, the least significant channel is that of the 'immaculate' subhaloes, I, which are subhaloes in $\mathcal{S}_{\rm f}$ that have no progenitor halo at $t_{\rm i}$. Either they formed as a host halo, and were subsequently accreted (all within the interval $\Delta t = t_{\rm f} - t_{\rm i}$), or they popped into existence as a subhalo. Since the latter is unphysical, it corresponds to a fluke of the (sub)halo finder or the merger tree algorithm. In particular, if the (sub)halo finder is unable to find the subhalo in more than four consecutive time-steps, then the phantom-patching (described in §2.2) fails and the subhalo will re-appear as an immaculate subhalo. In a time interval $\Delta t = 170\,{\rm Myr}$, the fractional contribution of immaculate subhaloes (averaged over the redshift range $0 < z < 0.06$), is only $\sim 10^{-4}$.

Fig. 3 shows the same $\Delta t = 170\,{\rm Myr}$ SEC fractions as in Fig.2, but this time as function of redshift. Except for the I and D channels, all SEC fractions are independent of redshift, at least over the small redshift range considered here ($z < 0.06$). The disruption channel is redshift independent for $z \gtrsim 0.018$, but then increases slightly towards $z = 0$. The reason for this behavior is discussed in detail in §4.5 below, but briefly, it arises because at low redshift there is not enough temporal information into the future to test whether the subhalo has disappeared from the catalog due to issues with the halo finder, or whether the disruption is real. The immaculate channel reveals a dramatic redshift dependence. There are zero immaculates in the nine `ROCKSTAR` halo catalogs with $z < 0.026$. However, at higher redshifts the fractional contribution of immaculates increases to almost 0.1% at $z = 0.05$. This redshift dependence arises from the fact that the `Consistent` merger tree algorithm of Behroozi et al. (2013b) removes subhaloes that are tracked for fewer than 10 time steps and never orbit outside of the virial radius of their host haloes. This effectively removes all immaculates from the halo catalogs in the outputs close to $z = 0$.

### 3.2 Dependence on Time Step

The fractions discussed above are all functions of host halo mass, $M_{\rm h}$, redshift, $z$, and the time-interval, $\Delta t$, between the simulation outputs. In the discussion above, we examined the dependencies on $M_{\rm h}$ and $z$ for fixed $\Delta t \sim 170\,{\rm Myr}$. We now focus on the dependence on $\Delta t$.

Using the 19 simulation outputs, we compute the various SEC fractions for all 171 different output pairs. Dividing by the time interval between the two outputs yields the fractional rate $\mathcal{R}_{\rm c} \equiv f_{\rm c}/\Delta t$, where 'c' can be any of the twelve SECs. We normalize these fractional rates by those for the last two outputs (corresponding to $z = 0.003$ and $z = 0$), and plot the resulting $\log[\mathcal{R}_{\rm c}/\mathcal{R}_{\rm c,0}]$ for each of the 171 different pairs as function of the corresponding $\Delta t$ in Fig. 4. Note that since the outputs are separated by almost identical time intervals, there are typically multiple output-pairs

that correspond to the same $\Delta t$ (i.e., there are $19-n$ pairs with $\Delta t \simeq n \times 42$ Myr, with $n = 1, 2, ...18$).

The transition channel, T, has a fractional rate that decreases precipitously with increasing $\Delta t$. This is simply a consequence of the fact that

$$f_{\rm T} = 1 - \sum_{\rm fwd \neq T} f_{\rm c} \qquad (2)$$

where the summation is over all forward channels other than T. Since the fractional contributions from all those channels increase with $\Delta t$, that of T must decrease.

The normalized, fractional rates for the accretion, ejection, and re-accretion channels are, to good approximation, independent of $\Delta t$. This indicates that their corresponding fractions are proportional to $\Delta t$. The fractional rates of stripping and merging, on the other hand, decrease with increasing $\Delta t$. As we discuss in §4.3, this is a consequence of the fact that the S and M channels are strongly correlated temporally, in that a subhalo that recently experienced stripping (merging) is more likely to experience merging (stripping). The same holds for the blossoming and withering channels, B and W.

Both the D and I channels reveal a dispersion in $\mathcal{R}_{\rm c}/\mathcal{R}_{\rm c,0}$ at fixed $\Delta t$. This is simply a manifestation of the redshift dependence of their fractions (see Fig. 3). Note that $\mathcal{R}_{\rm c,0} = 0$ for the immaculates, and we have therefore normalized its fractional rates by that for the *first* two outputs (corresponding to $z = 0.057$ and $z = 0.060$) instead. The resulting normalized rates decrease with increasing $\Delta t$, which arises from the fact that $f_{\rm I} = 0$ for $z < 0.026$ and strongly increases with redshift thereafter. In the case of disruption, $f_{\rm D}$ increases slightly towards $z = 0$. If we only include outputs at $z > 0.018$, for which $f_{\rm D}$ is independent of redshift, we find only a weak increase of the normalized, fractional disruption rate with increasing $\Delta t$.

Finally, the exchange channels $\rm X^+$ and $\rm X^-$ are 'composite' channels, in that they represent combinations of two events; either ejection combined with re-accretion, or accretion combined with stripping (cf. Fig. 1). Given that there is a characteristic time interval, $(\Delta t)_{\rm c}$, between these two events, we expect the fractional exchange rates to increase with $\Delta t$, until $\Delta t \gtrsim (\Delta t)_{\rm c}$, after which the fractional rate is expected to level out. The lower-right panels of Fig. 4 confirm this behavior, and suggest that $(\Delta t)_{\rm c} \sim 0.6$ Gyr. If we use the asymptotic rates for $\Delta t > 0.6$ Gyr as estimate of the effective rate at which subhaloes are exchanged among host haloes, and the take account of the weak halo mass dependence seen in Fig. 2, we infer fractional subhalo exchange rates of

$$\begin{aligned} \mathcal{R}({\rm X^+}) &= 0.011\ {\rm Gyr}^{-1} \left( \frac{M_{\rm h}}{10^{13}\, h^{-1}{\rm M}_\odot} \right)^{0.2} \\ \mathcal{R}({\rm X^-}) &= 0.008\ {\rm Gyr}^{-1} \left( \frac{M_{\rm h}}{10^{13}\, h^{-1}{\rm M}_\odot} \right)^{0.2} \end{aligned} \qquad (3)$$

Hence, over a Hubble time a few percent of subhaloes (and thus satellite galaxies) is expected to have changed their host halo. Note that the positive exchange rate (host gains a subhalo from another host) is slightly higher than the negative exchange rate (host looses a subhalo to another host). This is a consequence of the weak mass dependencies, and the fact that we have restricted ourselves to fairly massive host haloes with $10^{11.5}\ h^{-1}{\rm M}_\odot \leq {\rm M_h} \leq 10^{15}\ {\rm h}^{-1}{\rm M}_\odot$.

### 3.3 Mass Functions

An important diagnostic for the various SECs are their mass functions; both in terms of their instantaneous mass, $m$, and their mass at accretion, $m_{\rm acc}$. The blue and red curves in Fig. 5 show the cumulative subhalo mass functions for subhaloes residing in host haloes with $13.5 \leq \log[M_{\rm h}/(\,h^{-1}{\rm M}_\odot)] < 14.0$. Blue and red correspond to different epochs, $t_{\rm f}$ and $t_{\rm i}$, respectively, that are separated by 170 Myr. Clearly, over this time interval there is little to no *net* evolution in the subhalo mass function. The other curves indicate the mass functions of subhaloes associated with the various SEC channels, as indicated. Solid and dashed curves correspond to channels that add and remove subhaloes, respectively. Note that we have split the channels over two different panels in order to avoid clutter. The masses of the subhaloes, $m$, are normalized by the masses of their host haloes, $M$, while the vertical dotted lines corresponds to $m/M = m_{50}/10^{14}\, h^{-1}{\rm M}_\odot$, below which the cumulative mass functions start to asymptote due to the fact that our sample only includes subhaloes with $m \geq m_{50}$. We will discuss the mass functions of the various SEC channels below, when we discuss the individual channels in detail.

## 4 SUBHALO PROPERTIES ALONG INDIVIDUAL CHANNELS

Having discussed the fractional contributions of the various SECs to the evolution of subhaloes, we now take a closer look at subhaloes along each individual channel. In particular, we compare subhaloes following different SECs in terms of their orbits as well as their properties both at the present and at the epoch of accretion.

We characterize orbits using the specific orbital energy, $E = V^2/2 + \Phi(r)$, and the orbital angular momentum. Here $r$ is the halo-centric distance of the subhalo from the center of its host halo,

$$V = |\vec{v}_{\rm host} - \vec{v}_{\rm sub}| \qquad (4)$$

is the speed of the subhalo with respect to the center of its host halo, and $\Phi(r)$ is the potential energy at the location $r$ of the subhalo. We compute the latter assuming that the host halo is a spherical NFW (Navarro, Frenk & White 1997) halo, so that

$$\Phi(r) = -V_{\rm vir}^2\, \frac{\ln(1+cx)}{f(c)\, x}\,. \qquad (5)$$

Here $V_{\rm vir} = \sqrt{GM/r_{\rm vir}}$ is the circular velocity of the host halo at its virial radius, $x = r/r_{\rm vir}$,

$$f(x) = \ln(1+x) - \frac{x}{1+x}\,, \qquad (6)$$

and $c$ is the host halo's concentration parameter. Recall that subhaloes on unbound orbits ($E > 0$) are discarded from our sample (see §2.1).

The red histograms in Fig. 6 (reproduced, for comparison, in Figs. 7–10) show the distributions of a total of six properties for *all* subhaloes, independent of the SEC channel

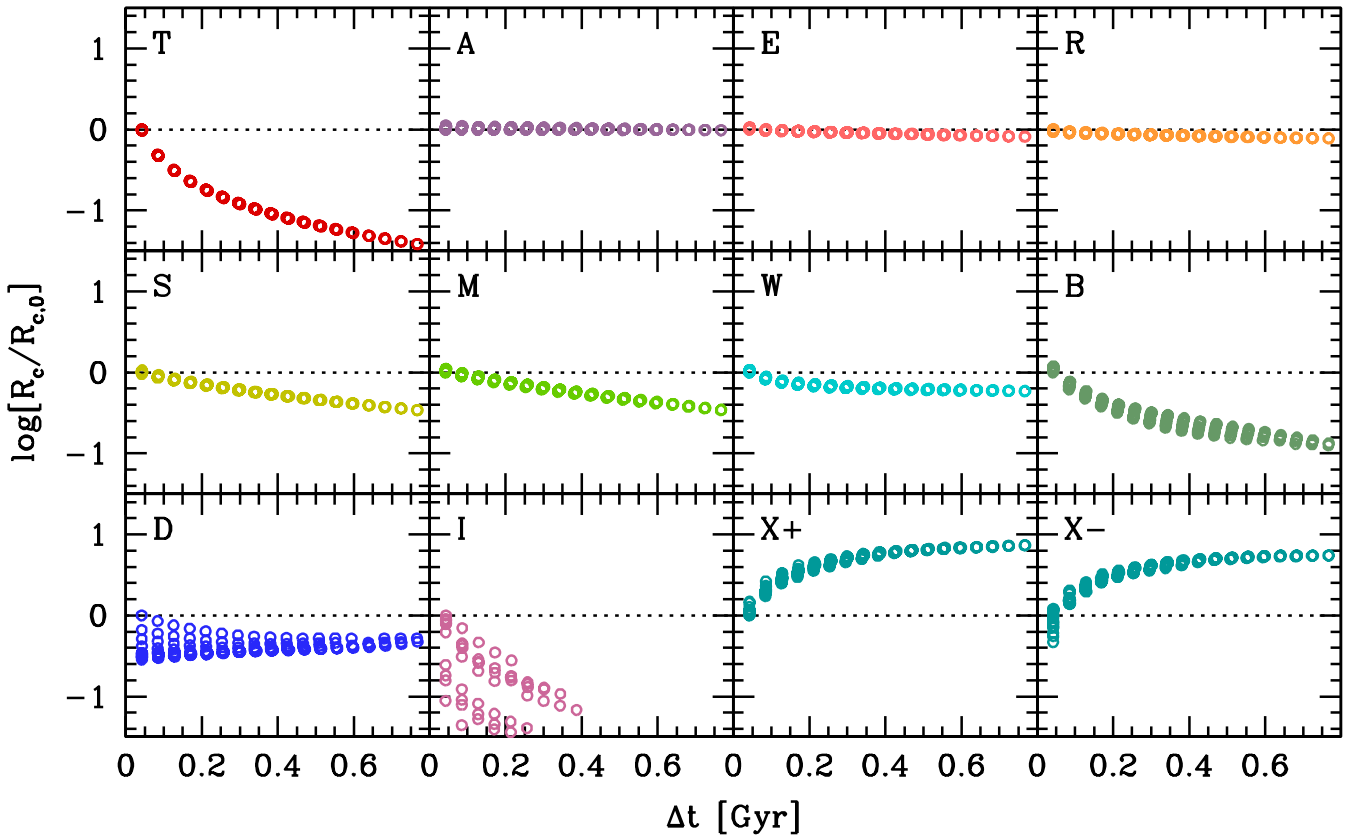


**Figure 4.** The logarithm of the normalized SEC rate (SEC fraction divided by the time interval, $\Delta t$, between two outputs, normalized by that between the final two outputs) as function of $\Delta t$ (in Gyr). Each panel corresponds to a different SEC, as indicated in the upper, left corner, and shows the results for all 117 output-pairs. If $R_{\rm c}/R_{\rm c},0 = 1$ for all $\Delta t$ it indicates a constant rate, and thus a fractional SEC contribution that increases linearly with $\Delta t$. Note that we have adopted the same color-coding as in Figs. 2 and 3.

to which they belong. From top-left to bottom-right these properties are:

- $r_{\rm c}(E)/r_{\rm vir}$, the radius of the circular orbit corresponding to the orbital energy $E$, expressed in terms of the virial radius of the host halo.
- $\eta$, the orbital circularity, defined as the ratio of the orbital angular momentum, $L$, and the angular momentum $L_{\rm c}(E)$ corresponding to a circular orbit of energy $E$. Radial and circular orbits have $\eta = 0$ and 1, respectively.
- $r/r_{\rm vir}$, the current halo-centric distance of the subhalo in units of the virial radius of the host halo.
- $z_{\rm acc}$ the redshift of accretion into the main progenitor of the current host halo.
- $m/m_{\rm acc}$, the ratio of the mass of the subhalo at the epoch under investigation to that at accretion.
- $K/|W|$, the virial parameter with $K$ and $W$ the total kinetic and potential energy of the subhalo. If the subhalo is in virial equilibrium with negligible surface pressure, then we expect that $K/|W| = 1/2$. Note that $W$ is computed ignoring any external potential, such as that from the host halo.

### 4.1 Subhaloes in Transition

By far the dominant SEC is the transition channel, T. For $\Delta t \simeq 42$ Myr more than 96 percent of the subhaloes evolve along this channel. Consequently, the properties of T subhaloes are virtually indistinguishable from those of *all* subhaloes, and are therefore well represented by the red histograms in Figs. 6–10. As is evident from the upper left-hand panel in those figures, a large fraction of T subhaloes are on orbits whose energy corresponds to a radius $r_{\rm c}(E)$ that is larger than the host halo's virial radius. Furthermore, T subhaloes are on orbits whose circularity, $\eta$, is strongly skewed towards more circular orbits. For an orbit with energy $E$ and angular momentum $L$ in a spherical potential, the peri-center, $r_{\rm p}$, and apo-center, $r_{\rm a}$, are the roots for $r$ of

$$\frac{1}{r^2} + \frac{2[\Phi(r) - E]}{L^2} = 0 \qquad (7)$$

(Binney & Tremaine 2008). Using the distributions of $E$ and $L$, we find that 59 percent of T subhaloes have $r_{\rm a} > r_{\rm vir}$ so that their orbit will take them beyond the host halo's (current) virial radius (i.e., they will at some point be 'ejected').

The distribution of halo-centric distances, $r/r_{\rm vir}$, is less centrally concentrated than what is expected for an NFW profile. This indicates that subhaloes are spatially anti-biased with respect to the dark matter distribution, a result that is well established (e.g., Ghigna et al. 1998, 2000; Gao et al. 2004; Diemand, Moore & Stadel 2004; Springel et al. 2008; Jiang & van den Bosch 2016b). The $z_{\rm acc}$ distribution is skewed towards small $z_{\rm acc}$, indicating that most surviving subhaloes, at any given time, have been accreted fairly recently (e.g., Zentner & Bullock 2003; Gao et al. 2004;

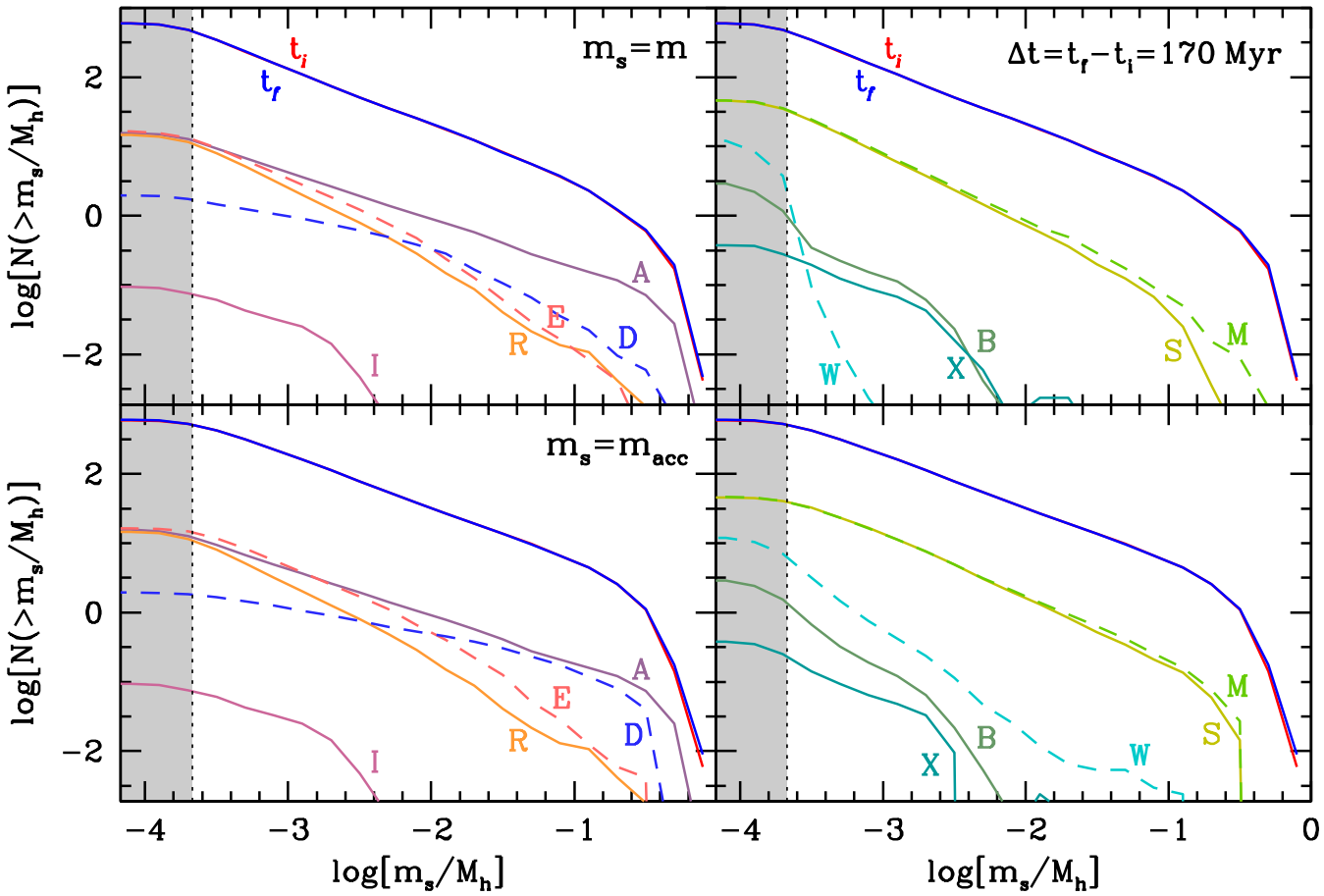


**Figure 5.** Cumulative mass functions for the various SECs for subhaloes that reside in host haloes with $13.5 \leq \log[M_{\rm h}/(h^{-1}{\rm M}_\odot)] \leq 14.0$ and for $\Delta t = t_{\rm f} - t_{\rm i} = 170\,{\rm Myr}$. Upper and lower panels show the results for the present-day (evolved) subhalo mass, $m$, and the mass at accretion, $m_{\rm acc}$, respectively, both normalized to $M_{\rm h}$. Solid and dashed curves correspond to channels that add and remove subhaloes, respectively. The grey-shaded regions mark where $m_{\rm s} < m_{50}$. Labeling and color scheme is the same as in all previous figures.

van den Bosch, Tormen & Giocoli 2005; Jiang & van den Bosch 2016a). We find that 50 percent of all $z = 0$ subhaloes in our sample have $z_{\rm acc} < 0.164$.

The $m/m_{\rm acc}$ distribution of subhaloes in the Bolshoi simulation is remarkably narrow. As is well known, the retained mass fraction $m/m_{\rm acc}$ is strongly correlated with $z_{\rm acc}$, in that haloes that were accreted earlier have experienced more mass loss, and thus have smaller $m/m_{\rm acc}$ (e.g., Gao et al. 2004; Zentner et al. 2005; van den Bosch et al. 2005, 2016). We find that 1.3 (0.02) percent of the subhaloes in our sample have $m/m_{\rm acc} < 0.1$ ($< 0.01$). As shown in Jiang & van den Bosch (2016a), the absence of subhaloes with small $m/m_{\rm acc}$, and thus large $z_{\rm acc}$, is mainly a consequence of subhalo disruption.

Finally, the distribution of the virial ratio is narrow, and centered around $K/|W| \simeq 0.5$, corresponding to virial equilibrium. The distribution is skewed towards higher values. As shown in van den Bosch et al. (2016), subhaloes experience a tidal shock near peri-center which temporarily boosts their $K/|W|$. Since the total binding energy of a dark matter subhalo is $E = K + W$, a virial ratio of $K/|W| > 1$ corresponds to a positive binding energy; i.e., a system that is likely to be close to tidal disruption. Among our sample of subhaloes, $\sim 0.9$ percent have $K/|W| > 1$.

### 4.2 Accretion, Ejection and Re-accretion

The accretion, ejection and re-accretion channels are closely related. In fact, they signal different events in the life of a typical subhalo (e.g., Lin, Jing & Lin 2003; Gill, Knebe & Gibson 2005; Sales et al. 2007; Ludlow et al. 2009). Accretion corresponds to the moment a subhalo enters the virial extent of its host halo, and if its orbital energy and angular momentum are conserved quantities, its orbit will once again take it outside of the host halo's virial radius ('ejection'). Hence, every subhalo is expected to be ejected again, unless either (i) the subhalo is disrupted during its first peri-centric passage, (ii) the subhalo experiences significant dynamical friction, or (iii) the host halo grows substantially during the orbital period, so that its virial radius becomes larger than the subhalo's apo-center. In fact, as we now demonstrate, all three processes play a role and have a dramatic impact on the freshly accreted population of subhaloes.

We start our discussion by comparing subhaloes at accretion and at ejection. As is evident from the lower-left panel of Fig. 6, subhaloes that are being ejected have a $z_{\rm acc}$ distribution that peaks around 0.25 (see also van den Bosch et al. 2016). Hence, at present there is on average about 3 Gyr between accretion and ejection.

The upper-left and upper-middle panels of Fig. 6 reveal

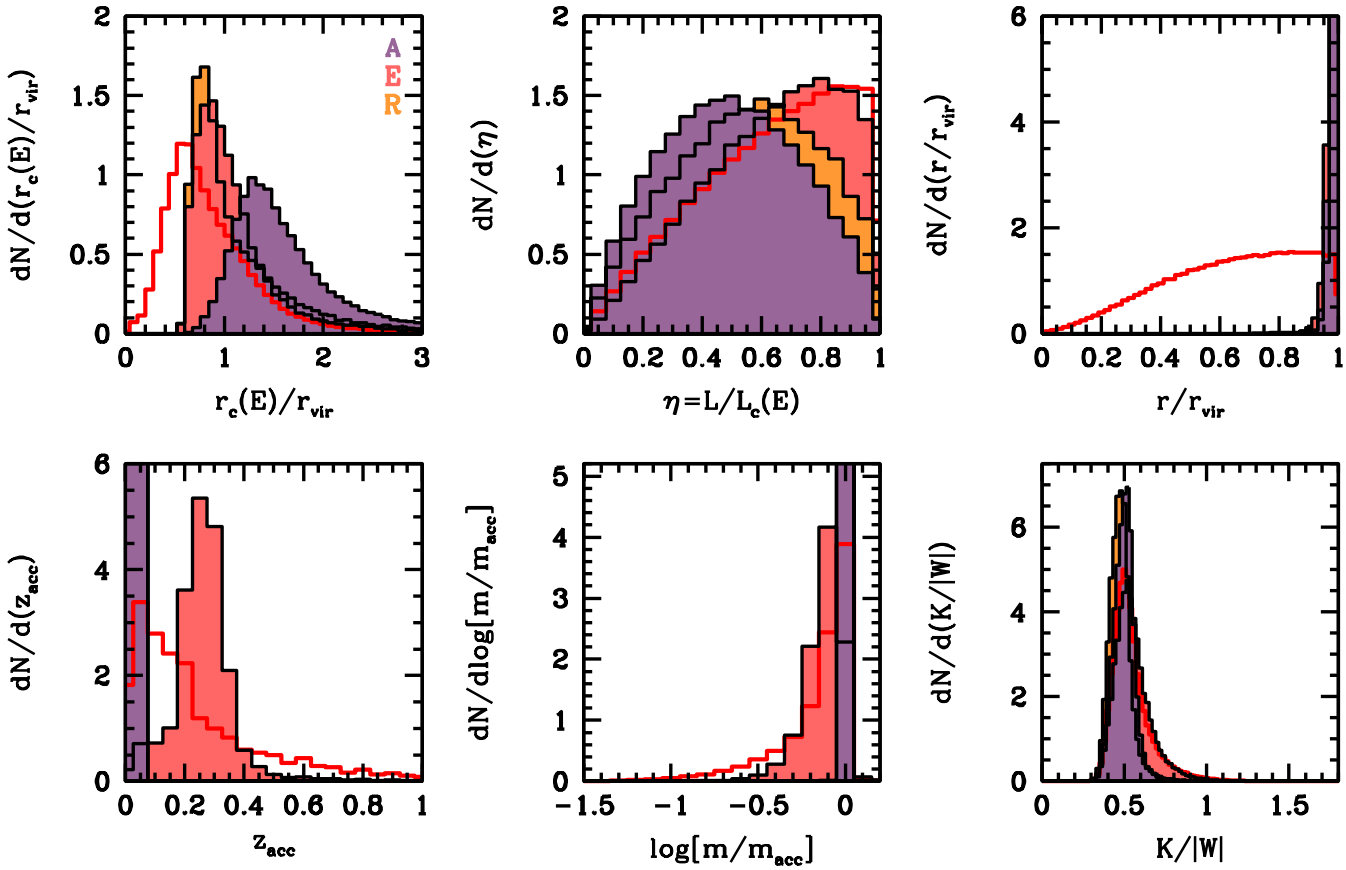


**Figure 6.** From left to right and top to bottom, the various panels show normalized distributions of the orbital energy expressed as $r_{\rm c}(E)/r_{\rm vir}$, orbital circularity $\eta$, instantaneous radius $r/r_{\rm vir}$, accretion redshift $z_{\rm acc}$, the logarithm of the mass ratio $m/m_{\rm acc}$, and the virial ratio $K/|W|$. Shaded histograms correspond to subhaloes belonging to the accretion channel, A, the ejection channel, E, and the re-accretion channel, R, as indicated, while the red histogram corresponds to *all* subhaloes, and is indistinguishable from that for transition (T) subhaloes. Note that, by definition, A and R subhaloes have $r \simeq r_{\rm vir}$ $m \simeq m_{\rm acc}$ and $z_{\rm acc}$ equal to the simulation output under consideration (all of which have $z < 0.06$.

a dramatic difference in the orbital properties of A and E subhaloes. Subhaloes at accretion have a broad, skewed distribution of $r_{\rm c}(E)/r_{\rm vir}$. The median is 1.26 and 11.2 percent of the A subhaloes have $r_{\rm c}(E)/r_{\rm vir} > 3$. For comparison, the median for E subhaloes is 1.0, while only $\sim 4$ percent have $r_{\rm c}(E)/r_{\rm vir} > 3$. The $\eta$ distributions are also very different. While that of subhaloes at accretion is remarkably symmetric around $\eta \sim 0.5$, in good agreement with previous studies (e.g., Tormen 1997; Zentner et al. 2005; Wetzel 2011; Jiang et al. 2015), the distribution of orbital circularities for subhaloes at ejection is strongly skewed towards more circular orbits. In fact, the $\eta$ distribution of $E$ subhaloes is very similar to that of *all* subhaloes. Note that this is contrary to naive expectations: subhaloes on more radial orbits (i.e., with smaller $\eta$), have larger apo-centric distances than orbits of the same energy with larger $\eta$. Hence, one might have expected that subhaloes with lower values of $\eta$ are more likely to experience ejection.

What causes this dramatic change in the orbital properties, over a time interval of only $\sim 3$Gyr? As shown in Wetzel (2011), the evolution in orbital parameters of accreting subhaloes between $z = 0.25$ and $z = 0$ is negligible. Hence, the differences are not a manifestation of evolution in the orbital properties at infall. Rather, they must reflect processes that occur inside the host halo. Using the average mass assembly histories of dark matter haloes (see van den Bosch et al. 2014), we infer that the average halo with mass in the range $10^{12}\,h^{-1}{\rm M}_\odot$ to $10^{15}\,h^{-1}{\rm M}_\odot$ grows its virial radius by about $20 \pm 5$ percent since $z = 0.25$. This effect by itself only explains about half of the difference in the $r_{\rm c}(E)/r_{\rm vir}$ distributions of A and E subhaloes, and has a negligible impact on the $\eta$-distribution (at least if the halo growth is adiabatic). Dynamical friction can drastically lower the orbital energy, but only for the most massive subhaloes, i.e., those with $m_{\rm acc}/M_{\rm h} \gtrsim 0.1$ (see discussion in van den Bosch et al. 2016). As is evident from Fig. 5, the mass function of subhaloes at accretion has a much larger fraction of massive subhaloes than that of the surviving or ejected subhaloes. Hence, dynamical friction plays an important role in reducing the orbital energies, and thus in lowering the average $r_{\rm c}(E)/r_{\rm vir}$. It also explains, at least partially, why subhaloes that are about to be ejected have larger circularities than orbits at accretion. As shown in van den Bosch et al. (1999), during peri-centric passage dynamical friction causes $\eta$ to increase. Note that the inverse is true at apo-center, where dynamical friction causes $\eta$ to decrease again resulting in little net change in $\eta$ when averaged over an entire radial orbit. However, since subhaloes between accretion and ejection

only experience a *peri*-centric passage, dynamical friction will cause a net shift in the distribution of orbital circularities to larger values (more circular orbits). The third effect that causes a large change in orbital properties between accretion and ejection is subhalo disruption. As we will show in §4.5 below, a significant fraction of newly accreted subhaloes is disrupted during their first peri-centric passage or shortly thereafter. Since subhaloes that are disrupted are preferentially on radial orbits, this helps to explain the pronounced deficit of small-$\eta$ orbits among the population of E (and T) subhaloes. To conclude, halo growth, dynamical friction and tidal disruption all play an important role in causing a dramatic change in the distribution of orbital properties of subhaloes between accretion and ejection.

As mentioned above, 59 percent of the surviving, present-day subhalo population in our sample have an apocenter $r_{\rm a} > r_{\rm vir}$, and are therefore expected to experience ejection. At first, this may seem inconsistent with the fact that the ratio $f_{\rm E}/f_{\rm A}$, averaged over host haloes with $10^{12.5} \leq M_{\rm h}/(h^{-1}\,{\rm M}_\odot) \leq 10^{14.5}$, is $1.0 \pm 0.02$, where the error reflects the scatter among different output-pairs separated by $\Delta t = 170$ Myr. However, the interpretation of the ratio $f_{\rm E}/f_{\rm A}$ is complicated by the fact that there are, on average, $\sim 3$ Gyrs between accretion and ejection during which the accretion rate of a host halo may undergo appreciable changes. Hence, one ought to compare the present-day ejection fraction to the accretion fraction at the (average) redshift at which those subhaloes were accreted ($z \simeq 0.25$). In general, the accretion rate of dark matter haloes declines with time (e.g., Neistein & Dekel 2008; Fakhouri, Ma & Boylan-Kolchin 2010; van den Bosch et al. 2014), which implies that the fraction of accreted subhaloes that is ejected is actually smaller than unity. Assuming that $f_{\rm A} \propto \dot{M}_{\rm h}/M_{\rm h}$, and using that $\dot{M}_{\rm h}/M_{\rm h} \propto (1+z)^{2.25}$ (Dekel et al. 2009), we have that $f_{\rm A}(z=0.25) \simeq 1.65 f_{\rm A}(z=0)$. Hence, $f_{\rm E}(z=0)/f_{\rm A}(z=0.25) \simeq 0.6$, which is in excellent agreement with the finding that 59 percent of present-day subhaloes have $r_{\rm a} > r_{\rm vir}$. The implication is that roughly 40 percent of the subhaloes that were accreted around $z = 0.25$ do not experience ejection; either because they were disrupted during their first peri-centric passage, or because of changes in their orbital properties.

The lower panel in the middle column of Fig. 6 shows that an average subhalo at ejection has already experienced significant mass loss since accretion; the average $m/m_{\rm acc}$ for E subhaloes in our sample is 0.77. This is not enough, however, to explain the large differences in the subhalo mass functions of A and E subhaloes evident from the upper panels of Fig. 5. Instead, as is evident from the lower panels, the E subhaloes already had a very different mass function at accretion. This clearly indicates that the subhaloes that do not experience ejection are predominantly the most massive subhaloes, which are the ones that experience the largest amount of dynamical friction.

Comparing the ejection and re-accretion fractions, we find that $f_{\rm R}/f_{\rm E} = 0.83 \pm 0.03$. If we assume that the ejection fraction evolves in the same way as the accretion fraction, i.e., $f_{\rm E} \propto \dot{M}_{\rm h}/M_{\rm h}$, then the relevant ratio is $f_{\rm R}(z=0)/f_{\rm E}(z=z_{\rm E}) \simeq 0.83(1+z_{\rm E})^{-2.25}$ where $z_{\rm E}$ is the average ejection redshift for subhaloes that are re-accreted at $z = 0$. This indicates that a significant fraction of subhaloes that is being ejected will not be re-accreted. We emphasize that this is not due to subhaloes having velocities that exceed the escape speed[‡]. After all, subhaloes on unbound orbits have been removed from our analysis. Hence, the fact that $f_{\rm R}(z=0)/f_{\rm E}(z=z_{\rm E}) < 1$ indicates that external tidal forces from neighboring haloes can have an appreciable impact on their orbit. In the extreme case, this may result in the subhalo being captured by another host halo, thus giving rise to subhalo 'exchange' (as reflected by the $\rm X^+$ and $\rm X^-$ channels). As is evident from Fig. 6, R subhaloes have orbital properties that are significantly different from those of E subhaloes, supporting the notion that external tides influence the orbital energy and/or angular momentum of subhaloes during their excursion outside of their host. The net effect is that R subhaloes are on more radial orbits than their E counterparts.

### 4.3 Stripping and Merging

Stripping, S, and merging, M, are each others inverse. Subhaloes in S transit from being a higher-order subhalo at $t_{\rm i}$ to a first-order subhalo at $t_{\rm f}$, while those in M transit from a first-order subhalo at $t_{\rm i}$ to a higher-order subhalo at $t_{\rm f}$. In principle, there are three effects that can contribute to stripping and merging: First of all, S and M could represent true 'physical' processes. For stripping, this corresponds to a higher-order subhalo being stripped off from its first-order parent halo by the tidal force of either the host halo or another subhalo, such that it is no longer bound to that parent. For merging this corresponds to two first-order subhaloes, initially unbound to each other, merging together such that the less massive one ends up on a bound orbit inside the more massive one. Secondly, merging followed by stripping can also be a manifestation of the ejection and re-accretion of higher-order subhaloes; similar to first-order subhaloes, 59 percent of which are on orbits with apo-centers that fall outside of their host halo, second-order subhaloes can be on orbits that take them temporarily outside of their (first-order) parent subhalo. This manifests itself as stripping followed by merging. And finally, stripping and merging may be manifestations of penetrating encounters, whereby two subhaloes that are unbound to each other, and with radial extents $R_1$ and $R_2$, have a close encounter with an impact parameter $b < {\rm MAX}[R_1, R_2]$.

In order to discriminate between these three possibilities, we now focus on the demographics of the S and M channels. Intriguingly, the fractions of subhaloes evolving, at any given instant, along the S and M channels are virtually identical. For the subhaloes in our sample we find that $f_{\rm S}/f_{\rm M} = 0.99 \pm 0.02$, where the average and standard deviation are taken over all 171 output pairs. Not only are their fractions identical, S and M subhaloes also have very similar mass functions (see Fig. 5), are on virtually identical orbits, and have indistinguishable properties (see Fig. 7). Comparing the properties of S and M subhaloes to those of all subhaloes, it is clear that S and M subhaloes are fairly representative of the full subhalo sample, except for their distri-

‡ Some subhaloes that are ejected from their host have experienced a three-body interaction that causes the subhalo to become unbound, and thus to escape without being re-accreted (e.g., Sales et al. 2007).

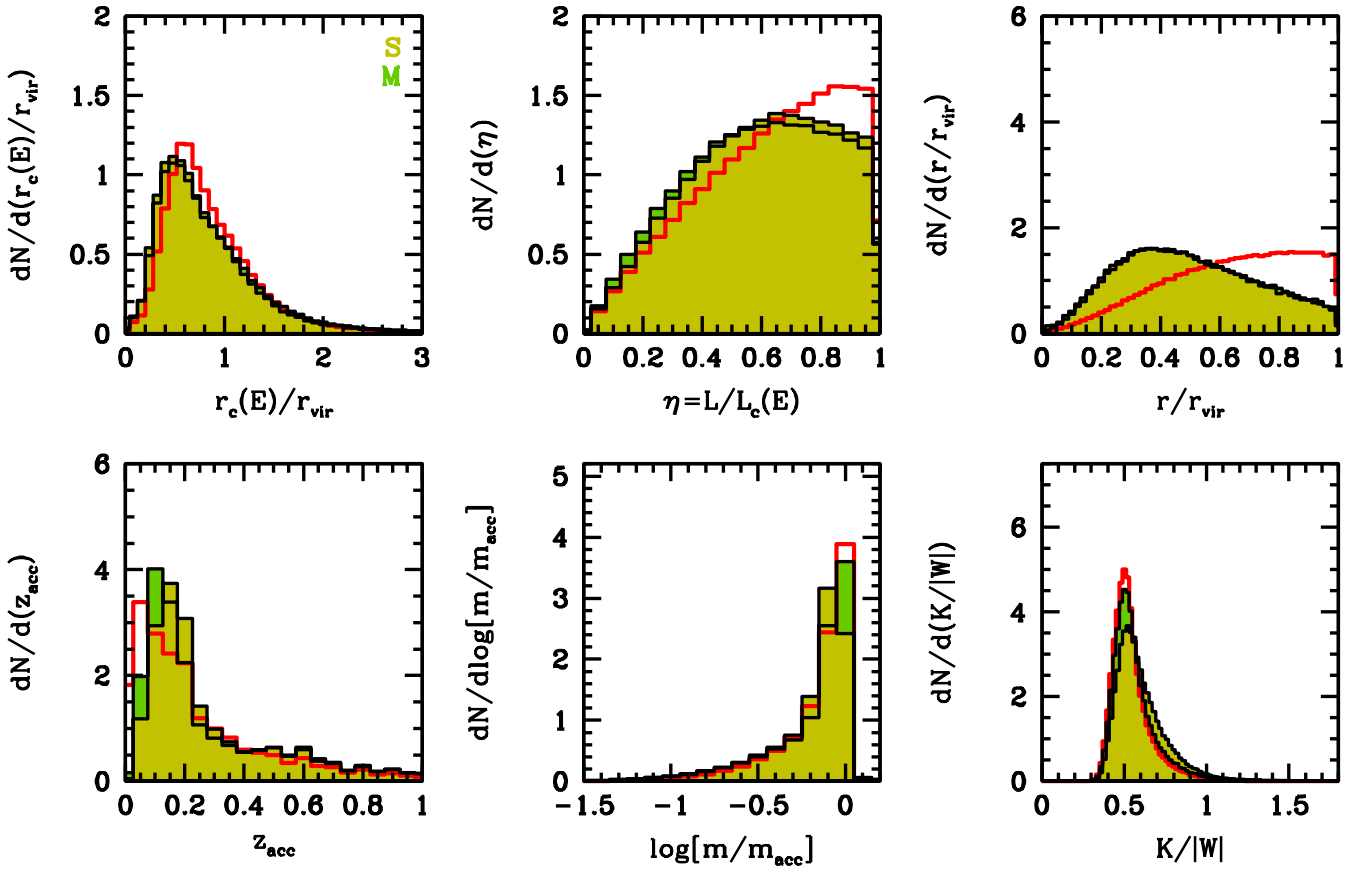


**Figure 7.** Same as Fig. 6, but for the stripping (S) and merging (M) channels. Note that S and M subhaloes are virtually indistinguishable. Their properties are also very similar to those of all subhaloes (red histogram), although their distribution of $r/r_{\rm vir}$ is clearly offset towards smaller halo-centric distances.

bution of halo-centric radii, $r/r_{\rm vir}$, which is clearly skewed towards smaller values. This indicates that stripping and merging preferentially occur closer towards the center of the host halo. S and M subhaloes also seem to avoid the most circular orbits (i.e., those with $\eta$ close to unity).

The fact that subhaloes along the S and M channels are virtually indistinguishable, and that stripping and merging occur at virtually identical rates, makes it extremely unlikely that the S and M channels represent physical stripping and merging of higher-order subhaloes. This is also supported by Fig. 4, which shows that $f_{\rm S}$ and $f_{\rm M}$ do not increase linearly with $\Delta t$, as would be expected if stripping and merging are independent physical processes. Rather, we find S and M to be strongly correlated temporally. A subhalo that merges between time steps $t_{n-1}$ and $t_n$, has a probability of being stripped between time steps $t_n$ and $t_{n+1}$ that is 6 times higher than for an average subhalo. As a consequence, we find that only 50 percent of subhaloes that merge between two outputs remain merged (i.e., are not stripped) for more than $\sim 0.3$ Gyr. This implies that the S and M channels do not correspond to actual stripping and merging (as defined above) of higher-order subhaloes. In addition, it also makes it unlikely that the majority of stripping and merging events are manifestations of the orbits of second-order subhaloes. After all, 0.3 Gyr is about an order of magnitude shorter than the typical orbital time between accretion (which manifests itself as merging) and ejection (which manifests itself as stripping).

Hence, the S and M channels most likely correspond to penetrating encounters between subhaloes. This is corroborated by Fig. 8, which compares the distributions of $V/V_{\rm max}$ for (second-order) S subhaloes (green histogram), and (first-order) T subhaloes (blue histogram). Here $V$ is the velocity of the subhalo with respect to its parent/host halo, whose maximum circular velocity is given by $V_{\rm max}$. As mentioned in §2.1, we exclude from our analysis any first-order subhalo that is not bound to its host halo. Consequently, the blue histogram, which cuts-off sharply around $V/V_{\rm max} \sim 2$, is representative of a population of bound subhaloes. The $V/V_{\rm max}$ distribution for S subhaloes is very different. It has a median of $V/V_{\rm max} = 5.2$, with 87.4 percent having $V/V_{\rm max} > 2$ (compared to 0.6 percent for T subhaloes); clearly, the vast majority of (second-order) S subhaloes are not bound to their (first-order) parent subhalo. We therefore conclude that the S and M channels are manifestations of high-speed penetrating encounters. In §5.2 we show that the inferred rate of penetrating encounters is remarkably high, which may have important ramifications for the evolution of subhaloes.

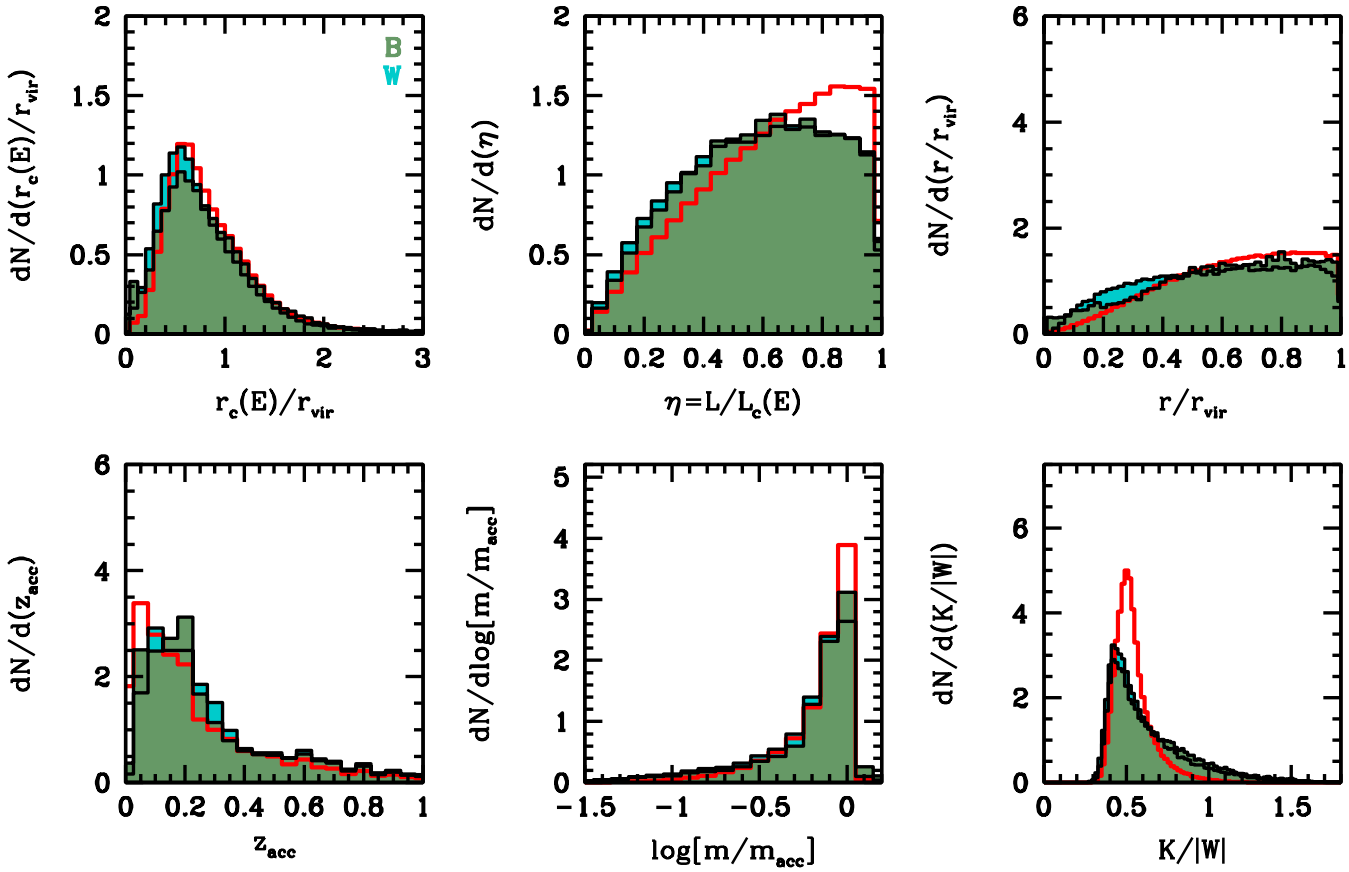


**Figure 9.** Same as Fig. 6, but for channels W and B.

### 4.4 Withering and Blossoming

Withering subhaloes, W, are defined as subhaloes whose mass drops below the 50 particle limit during the interval $\Delta t$. Blossoming is the inverse of withering, and B subhaloes therefore have their mass increase from below $m_{50}$ to above $m_{50}$. In general, one expects subhaloes to loose mass, and not gain mass, and thus for the B channel to be empty. Yet, we find that, in our fiducial time interval of $\Delta t \simeq 170$ Myr, about 0.6 percent of all subhaloes in our sample are blossoming. For comparison, in the same time interval roughly 2.3 percent of subhaloes wither.

Similar to S and M subhaloes, W and B subhaloes are strongly correlated temporally. Subhaloes that just blossomed are about 50× more likely to wither within the next 42 Myr than an average subhalo, while subhaloes that withered are $\sim 60\times$ more likely to have blossomed during the previous time step of 42 Myr. This explains why the normalized, fractional rates for the W and B channels, shown in Fig. 4 decrease with increasing $\Delta t$ (i.e., the fractions $f_{\rm W}$ and $f_{\rm B}$ do not increase linearly with $\Delta t$). Half of all subhaloes that blossom will wither again in $\sim 100$ Myr, while roughly 85 percent of withering subhaloes are gone from the sample indefinitely. The remaining 15 percent blossom again within about 100 Myr. All of this suggests that blossoming is mainly a manifestation of the mass histories of subhaloes being erratic, such that subhaloes with a mass close to $m_{50}$ repeatedly 'scatter' above and below this limit (see §5.1 below). If we interpret all blossoming as merely temporal fluctuations in $m(t)$, then we can correct the withering fraction by simply subtracting the blossoming fraction. This implies an effective, fractional withering rate of 0.10 Gyr$^{-1}$ (i.e., per Gyr roughly 10 percent of all subhaloes wither, without ever blossoming again).

As is evident from Fig. 9, withering and blossoming subhaloes have properties that are virtually indistinguishable from each other, and are very representative of an average subhalo. In particular, blossoming and withering do not preferentially occur along a particular subset of orbits, although they appear to 'avoid' the most circular orbits. There is also some indication that W subhaloes are, on average, at smaller halo-centric distances, consistent with the notion that mass loss is more prevalent closer to peri-center. In addition, W and B subhaloes have virial ratios, $K/|W|$, that are slightly more skewed towards larger values.

Finally, the right-hand panels of Fig. 5 show the cumulative mass functions of W and B subhaloes. Whereas withering subhaloes always have masses close to $m_{50}$, blossoming subhaloes can have masses that are quite substantial. In fact roughly 2 (0.2) percent of all B subhaloes in our sample have more than 100 (250) particles. If indeed, as argued above, blossoming subhaloes are a manifestation of noise in the subhalo mass assignment, this indicates that the error in the assigned subhalo mass can be disturbingly large. As we demonstrate in §5.1 below, this is indeed the case.

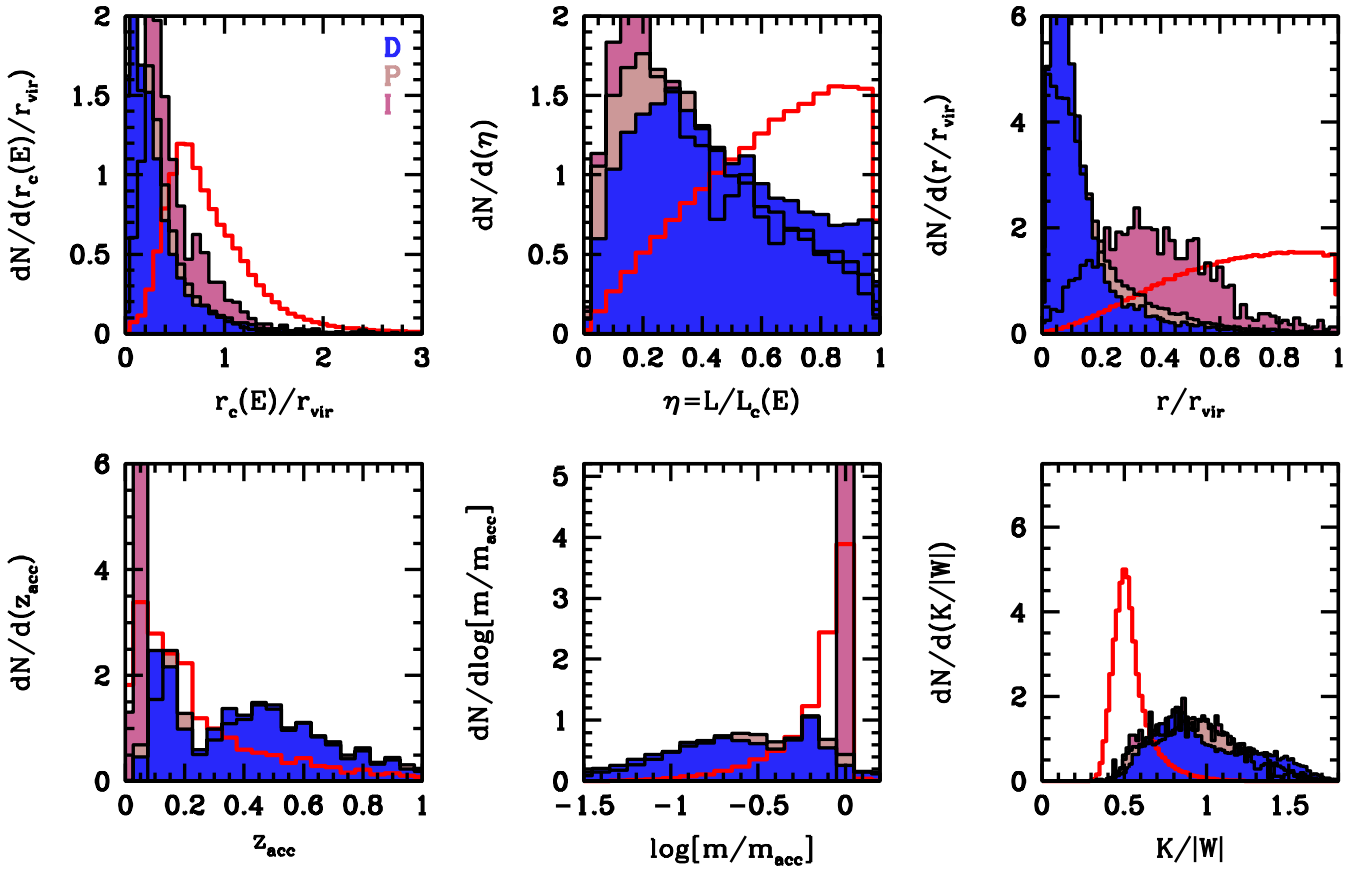


**Figure 10.** Same as Fig. 6, but for the disruption (D ) and immaculate (I ) channels, as well as for phantom subhaloes (P ).

### 4.5 Disruption, Phantoms and Immaculates

We now turn our attention to subhalo disruption. D subhaloes are defined as subhaloes that at $t_{\rm i}$ have a mass $m > m_{50}$, but that are not the most massive progenitor of their descendant halo. As discussed in §2.2, in the output before their disappearance from the halo catalogs, they experience a tidal acceleration $|\mathcal{T}| > 0.4\,{\rm km\,s^{-1}\,Myr^{-1}}$ comoving ${\rm Mpc}^{-1}$; subhaloes that disappear from the catalogs but that do not meet this tidal criterion are considered 'merger fluctuations' and are removed from the catalogs, together with all their progenitors at all previous time steps.

As is evident from Fig. 2 disruption rates are higher in less massive host haloes. This is consistent with expectations; subhaloes in lower mass hosts were accreted earlier, have experienced more mass loss on average, and are therefore more likely to be susceptible to disruption. In addition, less mass host haloes are more centrally concentrated, and therefore cause stronger tidal shocking. This latter effect is somewhat counter-balanced, though, by the fact that less massive hosts will accrete less massive subhaloes, which themselves are more concentrated, and hence more resilient to disruption.

Fig. 10 compares the properties of D subhaloes to those of immaculate subhaloes (I) and phantom subhaloes (P). Note that P subhaloes are not part of our complete set of evolution channels. Rather, phantoms are almost exclusively part of the T channel. All in all these D and P subhaloes have very similar properties. Their orbits are far more bound and radial than for an average subhalo (i.e., they have smaller $r_{\rm c}(E)/r_{\rm vir}$ and smaller $\eta$). Both D and P subhaloes are located at small halo-centric radii (54% of D subhaloes have $r/r_{\rm vir} < 0.1$, compared to 1% for T subhaloes), have elevated virial ratios (the median $K/|W| = 0.924$ for D subhaloes, compared to 0.521 for T subhaloes), and have clearly experienced more mass loss than an average subhalo. All of this is consistent with disruption being caused by the strong tidal field of the host halo near the orbit's peri-center.

The distribution of accretion redshifts for D subhaloes shows a pronounced absence at $z_{\rm acc} = 0$ and around $z_{\rm acc} \simeq 0.25$. Instead, D subhaloes have preferentially been accreted around $z_{\rm acc} \sim 0.15$ and 0.45. As shown in van den Bosch et al. (2016), subhaloes accreted at these redshifts are experiencing, on average, their first and second peri-centric passages around $z = 0$, whereas subhaloes accreted at $z \sim 0.25$ are currently experiencing their first apo-centric passage. Hence, this distribution of accretion redshifts is exactly what one expects if disruption occurs preferentially near peri-center.

The fact that phantom subhaloes have properties that are almost indistinguishable from D subhaloes raises the concern that the latter are actually phantoms, i.e., subhaloes that are not disrupted, but that temporarily disappear from the halo catalogs because of issues with the subhalo finder. Recall that a subhalo can only be assigned 'phantom status' for four consecutive time steps. Hence, if a subhalo fails detection in five or more consecutive time steps, it will show up in our sample as a disrupted subhalo. However, if dis-

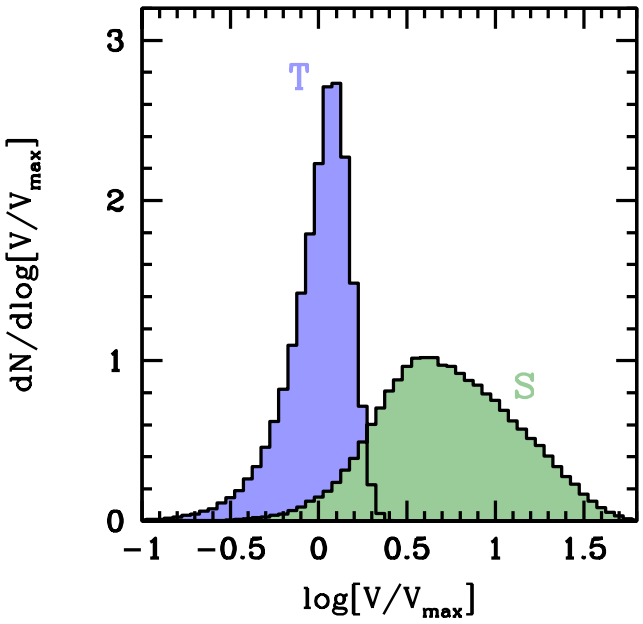


**Figure 8.** The green histogram shows the distribution of $\log[V/V_{\rm max}]$, where $V$ is the velocity of a second-order S subhalo (about to be stripped) with respect to its first-order parent halo, and $V_{\rm max}$ is the maximum circular velocity of that parent halo. For comparison, the blue histogram shows the distribution of $\log[V/V_{\rm max}]$ for T subhaloes with $V$ the velocity of the subhalo with respect to its host halo, and $V_{\rm max}$ the maximum circular velocity of that host halo. Since, by construction, all T subhaloes are bound, this is representative of the $V/V_{\rm max}$ distribution for a bound population. Clearly then, the vast majority of S subhaloes are not bound to their parent halo, indicating that S subhaloes are undergoing a penetrating encounter with another subhalo.

rupted subhaloes are really phantoms that are not traced long enough, then the majority of D subhaloes should have a corresponding I subhalo. However, the fraction of immaculates is much lower than that of D subhaloes ($f_{\rm I}/f_{\rm D} \lesssim 0.1$), indicating that at most a small subset of D subhaloes can be mis-classified phantoms (they don't really disrupt, they merely temporarily disappear from the halo catalogs). This is also supported by the left-hand panels of Fig. 5, which show that the mass function of D subhaloes is very different from that of I subhaloes.

However, there is one example where phantoms are clearly contributing significantly to the disruption channel, which is at $z \lesssim 0.012$. As shown in Fig. 3, disruption seems to become somewhat more prevalent at these low redshifts. However, this is entirely an artifact of contamination by phantom haloes, and arises from the fact that the simulation is only run to $z = 0$. Any subhalo that becomes a phantom in one of the final three outputs prior to $z = 0$ and is set to 'resurface' in the future (not covered by the simulation), ends up being (erroneously) identified as a disrupted subhalo. This explains the slight increase in the fraction of D subhaloes for $z \lesssim 0.012$.

As argued above, the fact that the fraction of immaculates is so much smaller than that of disrupted subhaloes indicates that the majority of disrupted subhaloes cannot be misclassified phantoms. However, it is still possible that the vast majority of immaculates are actually phantoms that simple weren't traced long enough. This is, in fact, supported by the fact that immaculates have orbital properties that are extremely similar to those of phantoms. As is evident from the upper right-hand panel of Fig. 10, immaculates are located at somewhat larger halo-centric radii than D and P subhaloes (but still much closer to the center than an average subhalo). This is exactly what is expected if immaculates are actually phantoms that resurface more than four time steps after they disappear, when sufficient time has passed since the last peri-centric passage. Therefore, we suspect that the majority of immaculates are actually phantoms that have been traced for an insufficient amount of time, and that their fraction will become even more insignificant if the merger tree algorithm would allow the creation of phantoms for more than four successive time steps.

## 5 THE TIDAL EVOLUTION OF DARK MATTER SUBHALOES

While orbiting their host halo, subhaloes experience dynamical friction, tidal stripping, and tidal heating during peri-centric passages and impulsive encounters with other subhaloes. All of these processes contribute to subhaloes loosing mass and/or being disrupted. This section takes a closer look at the demographics of tidal stripping and tidal disruption in the Bolshoi simulation. We start in §5.1 with a detailed examination of the tidal evolution of T subhaloes. We show that their mass and maximum circular velocity histories are extremely erratic, something that is difficult to reconcile with physical expectations. In §5.2 we derive an expression for the average time between penetrating encounters among subhaloes. Finally, in §5.3 we show that there are three distinct populations of disrupting subhaloes; a population that 'withers' below the mass resolution limit of the simulation, a population that 'merges' with the host, largely driven by dynamical friction, and a population that seems to abruptly disintegrate, something that again is difficult to reconcile with physical expectations.

### 5.1 Tidal Stripping

As shown in Jiang & van den Bosch (2016a), the (orbit-averaged) mass loss rate of dark matter subhaloes (in Bolshoi) is well described by

$$\frac{{\rm d}m}{{\rm d}t} = -0.86 \frac{m}{\tau_{\rm dyn}(t)} \left(\frac{m}{M}\right)^{0.07} \qquad (8)$$

where $\tau_{\rm dyn}(t)$ is the dynamical time of the host halo at time $t$, and $m$ and $M$ are the instantaneous masses of the subhalo and host halo, respectively (see also van den Bosch et al. 2005; Giocoli et al. 2010). The average half-mass time at $z = 0$ for a subhalo ranges from $\sim 2.5$ Gyr for the most massive subhaloes to $> 5.0$ Gyr for subhaloes that at accretion have a mass $m < 10^{-5}M$. On average, subhaloes accreted at $z_{\rm acc} \sim 0.32$ ($\sim 1.0$) have lost 50 (90) percent of their accretion mass at the present. For comparison, the maximum time interval examined in this study is only 0.81 Gyr, and subhaloes, on average, only loose a few percent of their mass over this period.

Note that Eq. (8) describes the orbit-averaged mass loss rates, averaged over the entire distribution of orbits and or-

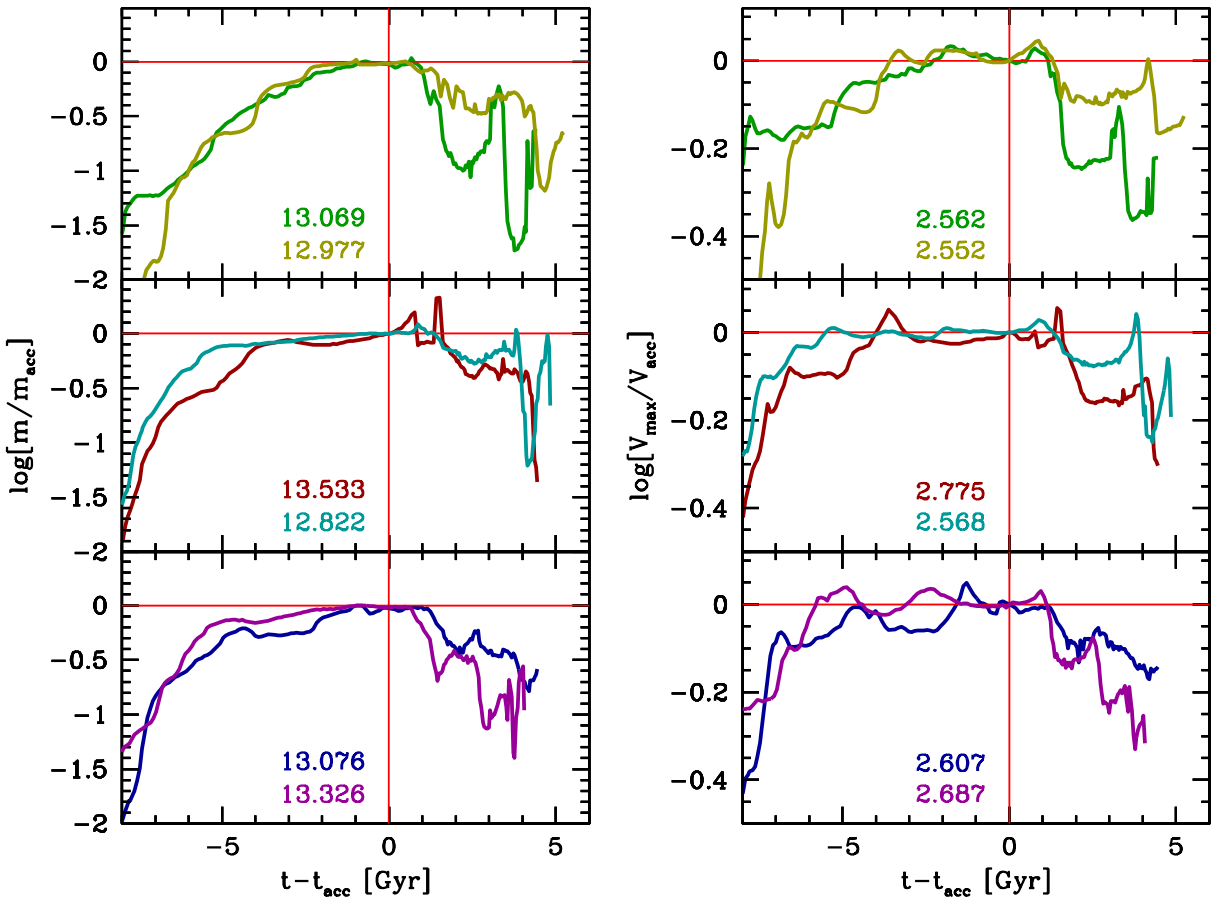


**Figure 11.** Mass (left) and $V_{\rm max}$ (right) histories for 6 subhaloes randomly selected from the Bolshoi simulation. To avoid crowding, we only show two histories per panel. The vertical, red line marks the epoch of accretion, $t_{\rm acc}$, after which the halo becomes a subhalo. The corresponding values of $\log[m_{\rm acc}/(h^{-1}\,{\rm M}_\odot)]$ and $\log[V_{\rm acc}/({\rm km\,s^{-1}})]$ are indicated in each panel. Note the large fluctuations in mass and maximum circular velocity that the subhaloes experience after accretion, which are very different from what is seen in analytical models and idealized simulations.

bital phases. In practice, because of the broad distributions of orbital properties and halo concentrations, one expects a fair amount of scatter in the instantaneous mass loss rates. In addition, analytical calculations of tidal stripping indicate that subhaloes loose the majority of their mass during the short periods associated with peri-centric passages, giving rise to 'stair-case' like behavior of $m(t)$ (e.g., Taylor & Babul 2001, 2004; Taffoni et al. 2003). This is indeed the behavior seen in idealized simulations of a single $N$-body subhalo orbiting within a fixed, analytical host halo potential (e.g., Hayashi et al. 2003; Peñarrubia et al. 2010). However, as we demonstrate next, this is not at all what is seen in the Bolshoi simulation.

Fig. 11 shows examples of the mass (left-hand panels) and $V_{\rm max}$ (right-hand panels) histories for 6 randomly selected subhaloes in the Bolshoi simulation. These were selected to have a mass at $z=0$ in excess of $10^{12}\,h^{-1}{\rm M}_\odot$ (i.e., more than 7400 particles). The histories are normalized to the mass and maximum circular velocity at the epoch of accretion, the logarithmic values of which are indicated in each panel. Note the 'noisy', jagged appearance of both $m(t)$ and $V_{\rm max}(t)$, which is very different from the 'stair-case like' behavior in analytical models and idealized simulations. It is well known that assigning masses to subhaloes can be tricky, especially if the subhalo is deeply embedded in the host halo (e.g., Muldrew, Pearce & Power 2011; Knebe et al. 2011; Han et al. 2012). In particular, it is extremely difficult to identify the outer boundary of the halo, which results in uncertainties in the assigned mass. However, the fact that the evolution in $V_{\rm max}$, which is a measure for the depth of the central potential well, is equally jagged as that in mass, suggests that this is not merely an issue related to identifying the subhalo's outer boundary.

The grey histograms of Fig. 12 plot the distributions of $\log[m(t+\Delta t)/m(t)]$ (left-hand panel) and $\log[V_{\rm max}(t+\Delta t)/V_{\rm max}(t)]$ (right-hand panel) for all subhaloes with present day mass $m_0 \geq 10^{12}h^{-1}\,{\rm M}_\odot$ and for all time-steps $t \rightarrow t+\Delta t$ with $\Delta t = 42$ Myr in which the halo is a subhalo. Positive and negative values correspond to an increase and decrease, respectively, in $m$ or $V_{\rm max}$. Note that the distributions are remarkably symmetric indicating that roughly half the time subhaloes actually *gain* mass, or increase their maximum circular velocity, at least according to the ROCKSTAR halo finder. More precisely, 40% (46%) of the time steps result in an *increase* of $m$ ($V_{\rm max}$). The dashed lines at the negative sides of the distributions are the mirror-reflections of the histograms at the positive sides, and are shown to highlight this high level of symmetry in the distri-

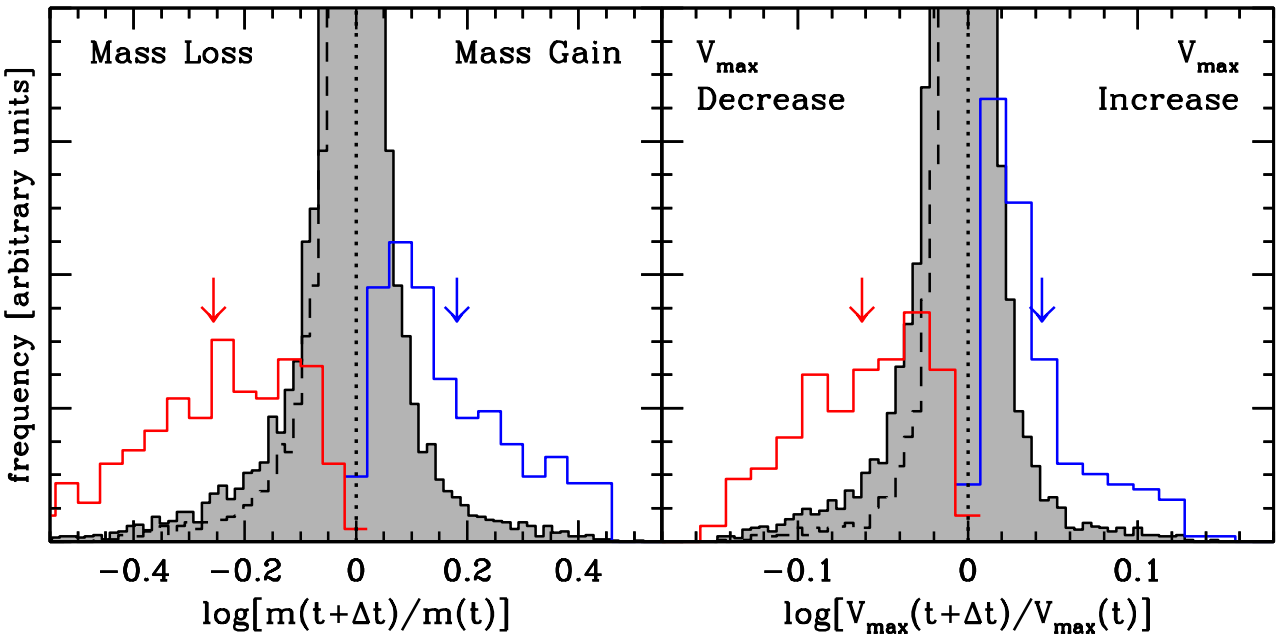


**Figure 12.** *Left-hand panel:* The shaded histogram plots the distribution of $\log[m(t+\Delta t)/m(t)]$ for all T-subhaloes with present day mass $m_0 \geq 10^{12}h^{-1}\,\mathrm{M}_\odot$ and for all time-steps $t \to t+\Delta t$ with $\Delta t = 42\,\mathrm{Myr}$ in which the halo is a subhalo. Positive and negative values correspond to mass gain and mass loss, respectively, as indicated. The dashed line at $\log[m(t+\Delta t)/m(t)] < 0$ is the mirror-reflection of the histogram for $\log[m(t+\Delta t)/m(t)] > 0$, and is shown to highlight the high level of symmetry in the distribution. The red and blue histograms indicate the distributions of the minimum and maximum $\log[m(t+\Delta t)/m(t)]$, respectively, for individual subhaloes. The vertical arrows indicate the corresponding medians. *Right-hand panel:* same as left-hand panel, but for $\log[V_{\rm max}(t+\Delta t)/V_{\rm max}(t)]$. See text for detailed discussion.

butions. In the case of subhalo mass, there is only a slight excess of mass loss over mass gain, and it is this slight excess that is responsible for the overall net mass loss experienced by subhaloes. Once again, this is very different from the stair-case-like behavior discussed above, for which $\log[m(t+\Delta t)/m(t)]$ only takes on negative values. For each subhalo we have determined both the minimum and maximum $\log[m(t+\Delta t)/m(t)]$ along their entire mass histories, the distributions of which are indicated by the red and blue histograms in Fig. 12, respectively. The vertical arrows indicate the corresponding medians. The median, extremal mass gain is $\log[m(t+\Delta t)/m(t)] = 0.18$, indicating that an average subhalo in the Bolshoi simulation, at some point after its accretion, in a time step of only 42Myr, increases its mass by 50 percent. Note also that the extrema-distribution extends well beyond $\log[m(t+\Delta t)/m(t)] = 0.3$; roughly 19 percent of all subhaloes experience time steps in which they more than double their own mass. The results for $V_{\rm max}$, shown in the right-hand panel, are qualitatively similar, with individual subhaloes revealing a median, extremal increase in $V_{\rm max}$ of a factor 1.1.

Are these jagged $m(t)$ and $V_{\rm max}(t)$ histories real, or are these artifacts of the simulations and/or the subhalo finder. One way in which a subhalo can fluctuate in mass is by experiencing a penetrating encounter with another subhalo (halo masses in `ROCKSTAR` are inclusive of all substructure). As discussed in §4.3, such penetrating encounters manifest themselves via the stripping (S) and merging (M) channels, and happen frequently. Since we only focus on first-order subhaloes, a penetrating encounter can at most boost the mass by a factor of two. Such equal-mass encounters, however, are extremely rare. By examining the mass ratios of subhaloes belonging to the M-channel, we find that only 0.97 (13.6) percent of the subhaloes that 'merge' contribute more than 10 (1) percent of mass to the subhalo into which they merge. Hence, penetrating encounters only make a very small contribution to the jaggedness of $m(t)$. Another way in which subhaloes can grow in mass, in principle, is by accreting smooth matter from their surroundings. However, as discussed and demonstrated in Han et al. (2012), subhaloes do not accrete any significant amount of matter from their host halo.

In order to gain some insight into the origin of the irregular, jagged behavior of $m(t)$ and $V_{\rm max}(t)$, the left-hand panel of Fig. 13 plots $\log[m(t+\Delta t)/m(t)]$ as function of $\Delta t$. As in Fig. 12, we consider all T subhaloes in our sample with a present-day mass $m_0 \geq 10^{12}\,h^{-1}\mathrm{M}_\odot$. The thick, solid curve indicates the median, while the shaded regions mark the 68, 95 and 99 percentile intervals. Over the 0.8 Gyr covered by our study, the average T subhalo only looses about 8 percent of its mass, but with a subhalo-to-subhalo variance that covers the range $0.27 < m(t+\Delta t)/m(t) < 1.85$ (99% interval). Most importantly, the positive (mass gain) wing of the $m(t+\Delta t)/m(t)$ distribution increases with $\Delta t$, at least up to $\Delta t \sim 0.4\,\mathrm{Gyr}$. This indicates that the episodes of (strong) subhalo mass increase are coherent over timescales of $\Delta t \sim 0.4$ Gyr; this coherence is also evident from the mass histories shown in Fig. 11.

The right-hand panel of Fig. 13 plots the distributions of halo-centric radii within the host halo, $r/r_{\rm vir}$, at which the subhaloes experience time-steps of $\Delta t = 42$ Myr in which $\log[m(t+\Delta t)/m(t)] > +0.2$ (extreme mass gain; red his-

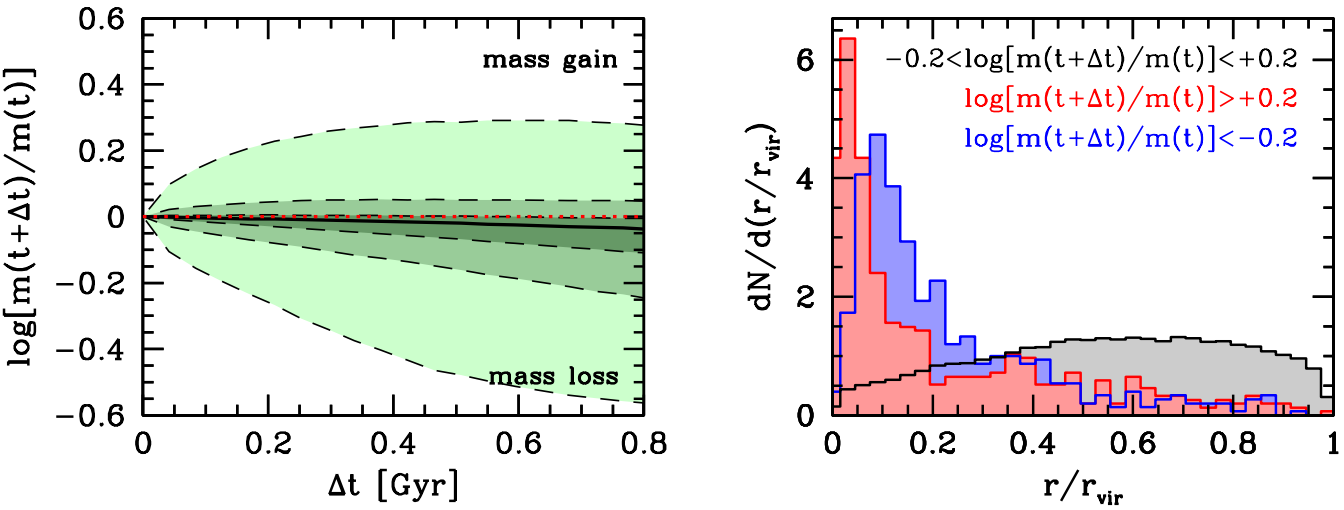


**Figure 13.** *Left-hand panel:* The ratio $m(t+\Delta t)/m(t)$ as function of $\Delta t$ for all T subhaloes in our sample with $m_0 > 10^{12}h^{-1}\,\mathrm{M}_\odot$. The thick, solid black line indicates the median, while the shaded regions mark the 68, 95 and 99 percentiles. The red, dotted line indicates $m(t+\Delta t)/m(t) = 1$ and is shown for comparison. As in Fig. 12 positive and negative values of $\log[m(t+\Delta t)/m(t)]$ correspond to mass gain and mass loss, respectively, as indicated. *Right-hand panel:* The distribution of halo-centric radii where subhaloes experience different amounts of mass loss or gain, as indicated. Note that episodes of extreme mass loss and mass gain preferentially occur at small halo-centric radii.

togram), $\log[m(t+\Delta t)/m(t)] < -0.2$ (extreme mass loss; blue histogram), and $-0.2 < \log[m(t+\Delta t)/m(t)] < +0.2$ (modest change in mass; black histogram). Clearly, extreme mass loss and gain occurs preferentially at small halo-centric radii. This is expected for the mass loss, which, as discussed above, peaks during peri-centric passage. However, the episodes of extreme mass gain, which typically occur at even smaller halo-centric radii, are not expected. As shown in Han et al. (2012), subhaloes can re-accrete some of their own matter that was stripped off at earlier times. In particular, during a peri-centric passage a subhalo experiences a drastic drop in mass, followed by a short period in which it 're-accretes' some of this mass. Physically, this can come about because the tidal stripping and shocking has pushed the subhalo out of virial equilibrium; consequently, the subhalo undergoes re-virialization, which can in principle rebind some of the particles that immediately after the impulsive shock have positive binding energy. However, as discussed in van den Bosch et al. 2016, in prep.), the magnitude of this physical 're-binding' is expected to be very small (few percent increase in mass at most), much smaller than the mass growth episodes evident in Fig. 11.

We are left to conclude that the jaggedness in $m(t)$ and $V_{\rm max}(t)$ most likely reflects serious problems with the subhalo finder. As demonstrated by Han et al. (2012), the detailed $m(t)$ in numerical simulation during a peri-centric passage is extremely sensitive to details regarding the unbinding algorithm used as part of the subhalo finder: in particular, the AMIGA Halo Finder (AHF; Knollmann & Knebe 2009) and `ROCKSTAR` typically yield larger 'fluctuations' in $m(t)$ during peri-centric passage than the Hierarchical Structure Finder (HSF; Maciejewski et al. 2009) or the Hierarchical Bound-Tracing (HBT; Han et al. 2012) algorithm. Hence, we conclude that the fluctuations in subhalo mass and maximum circular velocity reflect problems with the `ROCKSTAR` subhalo finder, which become extreme whenever the subhalo is located close to the center of its host halo. Similar studies are required to examine how other subhalo finders fair in this respect.

Finally, although individual subhaloes may occasionally carry very substantial errors in their instantaneous mass and/or maximum circular velocity, in Appendix A we show that this does not introduce an appreciable, systematic error in the inferred subhalo mass or $V_{\rm max}$ functions.

### 5.2 Rate of Penetrating Encounters

As we have seen in §4.3, the stripping and merging channels are mainly manifestations of penetrating encounters among subhaloes. Here a penetrating encounter is defined as having an impact parameter $b < \max(R_1, R_2)$, with $R_1$ and $R_2$ the radii of the subhaloes involved in the encounter. In this section we derive a simple estimate for the rate of such penetrating encounters.

Let $\tau_{\rm enc}(m_0)$ be the mean time for a subhalo of mass $m_0$ between two penetrating encounters with subhaloes of mass $m > m_0$. For a subhalo, the cross section for a penetrating encounter, $\sigma$, is independent of its velocity with respect to the host halo, $v$. Hence,

$$\tau_{\rm enc}(m_0) = \frac{1}{n\,\langle\sigma\rangle\,\langle v\rangle}\,, \qquad (9)$$

where $n$ is the number density of subhaloes with $m > m_0$. As shown by Gao et al. (2004) , the subhalo abundance *per unit halo mass* is roughly $\mathrm{d}n/\mathrm{d}m \propto m^{-1.9}$, with a normalization that is independent of host halo mass (see also van den Bosch et al. 2005). The interaction cross section $\sigma = \pi R^2$ where $R$ is the radius of the more massive subhalo. Assuming that the size of a subhalo of mass $m$ is proportional to $m^{1/3}$, we thus have that $\sigma \propto m^{2/3}$. Averaging over all subhaloes of mass $m > m_0$ one finds that

$$n\,\langle\sigma\rangle = \frac{M}{V}\int_{m_0}^{M}\frac{\mathrm{d}n}{\mathrm{d}m}\sigma(m)\,\mathrm{d}m \propto m_0^{-0.23}\,, \qquad (10)$$

where we have used that, according to the halo virial relations, the volume of a halo $V \propto M$, and we have assumed that $m_0 \ll M$. Finally, using that $\langle v \rangle \propto M^{1/3}$, we obtain that

$$\tau_{\rm enc}(m_0) \propto M^{-1/3}\, m_0^{0.23}\,. \qquad (11)$$

When considering all subhaloes of mass $m_0 > m_{\rm min}$, the average time between penetrating encounters is simply

$$\langle \tau_{\rm enc} \rangle \propto M^{-1/3}\, m_{\rm min}^{0.23} \qquad (12)$$

Let $f_{\rm M}$ be the fraction of subhaloes that evolve along the merging channel in a time interval $\Delta t$. Since merging is merely a manifestation of penetrating encounters with other, *more massive* subhaloes (see §4.3), we have that $\langle \tau_{\rm enc} \rangle = \Delta t/f_{\rm M}$, as long as $\Delta t$ is sufficiently small so that we can ignore multiple encounters per subhalo (i.e., as long as $f_{\rm M} \ll 1$). Using the smallest time-step available for the Bolshoi simulation ($\Delta t = 42$ Myr), we find that $f_{\rm M}$ increases from $\sim 0.006$ for $M = 10^{12}\ h^{-1}{\rm M}_\odot$ to $\sim 0.05$ for $M = 10^{15}\ h^{-1}{\rm M}_\odot$. Note that this scaling with host halo mass is in excellent agreement with our simple estimate of Eq. (12), according to which $\langle \tau_{\rm enc} \rangle \propto M^{-1/3}$. Using that $f_{\rm M}$ corresponds to a minimum subhalo mass of $m_{\rm min} = m_{50} = 6.75 \times 10^9\ h^{-1}{\rm M}_\odot$, we infer an average time in between two penetrating encounters of

$$\langle \tau_{\rm enc} \rangle \simeq (5 \pm 0.5)\, M_{12}^{-1/3} \left( \frac{m_{\rm min}}{10^9\ h^{-1}{\rm M}_\odot} \right)^{0.23} {\rm Gyr}\,, \qquad (13)$$

where $M_{12}$ is the host halo mass in units of $10^{12}\ h^{-1}{\rm M}_\odot$. The above can be recast as

$$\langle \tau_{\rm enc} \rangle \simeq (3 \pm 0.3)\, M_{12}^{-0.1} \left( \frac{m_{\rm min}/M}{10^{-4}} \right)^{0.23} {\rm Gyr}\,. \qquad (14)$$

Note that both of these expressions are only valid at $z \sim 0$ and for $m_{\rm min}/M \ll 1$.

Comparing the mean free time, $\langle \tau_{\rm enc} \rangle$, to the host halo's dynamical time $\tau_{\rm dyn} = \sqrt{3\pi/16 G\bar{\rho}} \simeq 3.1\,{\rm Gyr}$ it is clear that penetrating encounters of subhaloes with more massive subhaloes is extremely common (see also Tormen et al. 1998). In particular, subhaloes with a mass $m = 10^8\ {\rm M}_\odot$ orbiting inside a Milky-Way size host halo have on average about one penetrating encounter with another, more massive subhalo per dynamical time. Since the majority of these encounters are high speed (see Fig. 8), it is clear that impulsive encounters among subhaloes may play an important role in their evolution (see also Moore et al. 1996).

### 5.3 Tidal Disruption

The combined impact of tidal stripping and tidal heating can result in the complete disruption of a subhalo. Indeed, one of the evolution channels identified in this work is the disruption channel D. Although disruption may appear insignificant, given that the fractional contribution shown in §3.1 is only $\sim 0.5$ percent, be aware that this is the fractional contribution for a short time interval of $\Delta t = 170\,{\rm Myr}$. As is evident from Fig. 4, to good approximation $f_{\rm D} \propto \Delta t$, which implies a disruption rate of 2.4 percent per Gyr. It is important to stress that this only accounts for subhaloes that at the moment of disruption have a mass $m \geq m_{50}$. There are also subhaloes that disrupt after first experiencing mass loss to (well) below $m_{50}$. As discussed in §4.4, the effective rate at which this occurs is given by the difference between the withering (W) rate and the blossoming (B) rate, and is roughly 0.10 Gyr$^{-1}$. Hence, if we include this effective withering as an additional disruption channel, the total disruption rate in the Bolshoi simulation amounts to $\sim 13$ percent per Gyr.

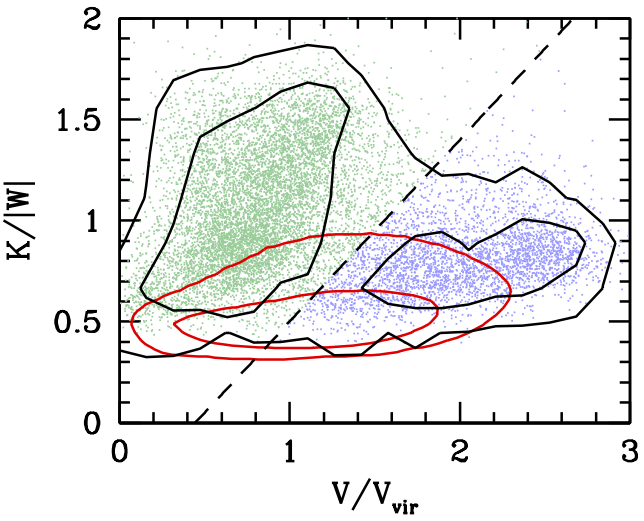


**Figure 14.** The distribution of disrupting subhaloes in the parameter space of the virial ratio $K/|W|$ versus the ratio $V/V_{\rm vir}$, which is the instantaneous velocity of the subhalo with respect to its host halo in units of the host halo's virial velocity. The black contours indicate the 68 and 95 percentiles of this distribution, which is clearly bimodal. The dashed line marks the critical virial ratio $(K/|W|)_{\rm crit}$ (Eq. [15]), which is used to separate D-subhaloes into two categories: ${\rm D_m}$ (green dots), which have a virial ratio larger than $(K/|W|)_{\rm crit}$, and ${\rm D_d}$ (blue dots) for which $K/|W| < (K/|W|)_{\rm crit}$. For comparison, the red contours indicate the 68 and 95 percentiles of the distribution of T-subhaloes in $(K/|W|, V/V_{\rm vir})$-space.

Indeed, as shown in Jiang & van den Bosch (2016a,b), subhalo disruption is prevalent in the Bolshoi simulation: of all subhaloes accreted at $z_{\rm acc} = 1$ (2), with a mass $m_{\rm acc} > 10^{-4} M_0$ (here $M_0$ is the present-day mass of the host halo), only about 35 (10) percent survive to the present day. And when only considering the more massive subhaloes with $m_{\rm acc}/M_0 > 0.01$ ($> 0.1$) the surviving fractions drop to roughly 20 (5) percent for an accretion redshift of $z_{\rm acc} = 1$. It is interesting to compare these survival fractions with predictions based on a disruption rate of 0.13 Gyr$^{-1}$. Using that the look-back time to $z = 1$ for the Bolshoi cosmology is 7.8 Gyr, the expected survival fraction for subhaloes accreted at $z_{\rm acc} = 1$ is equal to $0.87^{7.8} = 0.34$, in excellent agreement with the survival fraction quoted above and taken from Jiang & van den Bosch (2016a,b)

Based on these numbers, it appears that subhalo disruption is an extremely important dynamical process. However, it is prudent to be wary of numerical artifacts. After all, it is well known that limiting mass and/or force resolution can artificially erase substructure. In fact, this is the reason why it took until 1996 for numerical simulations to start resolving substructure in dark matter haloes (e.g., Moore et al. 1996; Tormen et al. 1997; Klypin et al. 1999). In the Bolshoi simulation, the contribution of the W channel to the

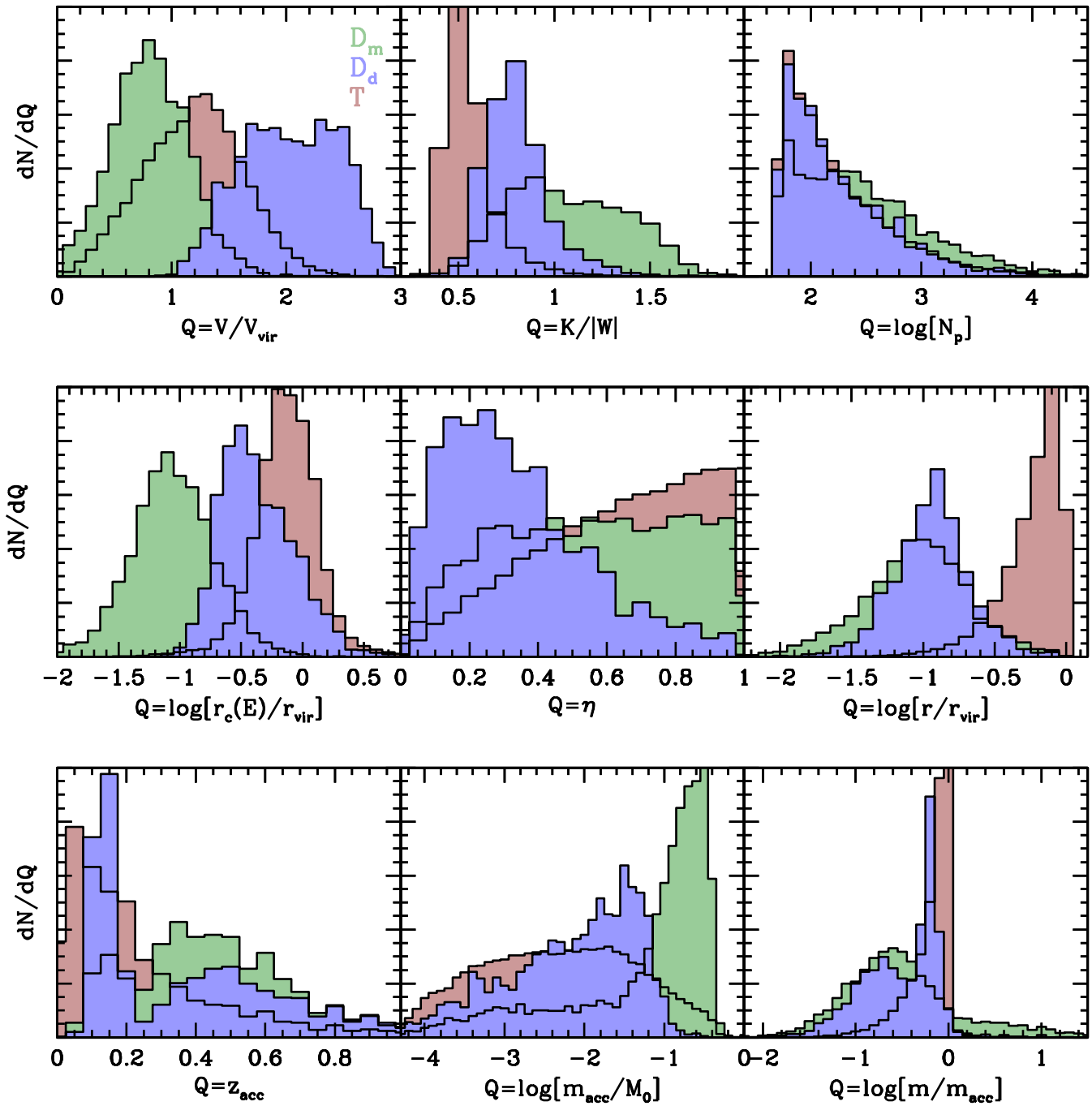


**Figure 15.** Statistics of D subhaloes. Each panel shows the (normalized) distributions of various subhalo properties for $D_m$ subhaloes (green histograms), $D_d$ subhaloes (blue histograms) and, for comparison, T subhaloes (red histograms). From top-left to bottom right, these subhalo properties are $V/V_{\rm vir}$, the virial ratio $K/|W|$, the instantaneous number of subhalo particles, $N_{\rm p}$, the orbital energy as expressed via $r_{\rm c}(E)/r_{\rm vir}$, the orbital circularity, $\eta$, the instantaneous halo-centric radius normalized by the host halo's virial radius, $r/r_{\rm vir}$, the subhalo's accretion redshift, $z_{\rm acc}$, its mass at accretion normalized by the present-day host halo mass, $m_{\rm acc}/M_0$, and the remaining mass fraction, $m/m_{\rm acc}$. Note the distinct demographics of $D_m$ and $D_d$ subhaloes.

disruption rate is almost certainly numerical, as it is clear that limiting mass resolution affects the subhalo mass function for $m < m_{50}$. For the actual disruption channel, D, though, mass resolution seems to be of little concern. As is evident from the left-hand panels of Fig. 5, the mass function of D subhaloes clearly is *not* skewed towards low mass haloes; rather, it is the channel with the mass function that is most heavily skewed towards the massive end (with the possible exception of the accretion channel A).

### *5.3.1 Demographics of subhalo disruption*

In order to get insight as to the cause of subhalo disruption in the Bolshoi simulation, we now examine subhaloes

in the D-channel in detail. In what follows, we exclude D subhaloes at $z < 0.012$ since, as discussed in §4.5, these are contaminated with phantoms, though we have verified that including them makes no substantial difference.

Fig. 14 plots the virial ratio $K/|W|$ of D-subhaloes as a function of $V/V_{\rm vir}$, the instantaneous velocity of the subhalo with respect to its host halo in units of the host halo's virial velocity. The black contours indicate the 68 and 95 percentiles of the distribution, which is clearly bimodal, suggesting that there are two distinct populations of D-subhaloes. For comparison, the red contours mark the 68 and 95 percentiles of the $(K/|W|, V/V_{\rm vir})$-distribution of T subhaloes. The dashed line roughly separates the two categories of disrupting subhaloes, and is specified by

$$(K/|W|)_{\rm crit} = 0.9(V/V_{\rm vir}) - 0.4 \quad (15)$$

In what follows we refer to subhaloes with a virial ratio $K/|W|$ larger and smaller than $(K/|W|)_{\rm crit}$ as $\rm D_m$ and $\rm D_d$ subhaloes, respectively, where the subscripts refer to 'merging' and 'disintegration'. Although this particular split in $(K/|W|, V/V_{\rm vir})$-space is somewhat arbitrary, we show below that $\rm D_m$ and $\rm D_d$ subhaloes are clearly distinct. In addition, we have verified that none of our results are sensitive to small changes in Eq. (15).

As is evident from Fig. 14, $\rm D_m$ subhaloes have relatively high virial ratios (median $K/|W| = 1.06$), and low host-halo-centric velocities. As we show below, $\rm D_m$ subhaloes are 'merging' with the host halo; they loose their identity in that they can no longer be discriminated from host halo particles in phase-space. Mainly due to dynamical friction, these subhaloes have become submerged in the background that is the center of their host halo. Roughly 70 percent of all D-subhaloes (corresponding to a fractional rate of 0.02 $\rm Gyr^{-1}$) fall in this sub-category. The other 30 percent (corresponding to a fractional rate of 0.009 $\rm Gyr^{-1}$) are $\rm D_d$ subhaloes, which, at the moment of disruption, have high host-halo-centric velocities, and virial ratios that are only slightly higher than for T-subhaloes. We (provisionally) interpret these as subhaloes that 'disintegrate' due to tidal heating and stripping. However, as we demonstrate below, their behavior and demographics are difficult to reconcile with these physical process, and we suspect instead that their disruption is a numerical artifact.

Fig. 15 compares the distributions of nine different parameters for $\rm D_m$ subhaloes (green histograms), $\rm D_d$ subhaloes (blue histograms) and T subhaloes (red histograms). The left and middle panels of the upper row show the distributions of $V/V_{\rm vir}$ and $K/|W|$, which are the two parameters that were used to split D-subhaloes in its two categories. Hence, it is not surprising that $\rm D_m$ and $\rm D_d$ subhaloes appear distinct with respect to these two parameters. However, most of the other parameters also reveal clear differences. For example, whereas the distribution of the number of particles, $N_{\rm p}$, (upper left-hand panel) of $\rm D_d$ subhaloes is virtually indistinguishable from that of T subhaloes, that of $\rm D_m$ subhaloes is offset to significantly larger values; i.e., $\rm D_m$ subhaloes are more massive than an average subhalo. This is also evident from the $m_{\rm acc}/M_0$ distributions, shown in the middle panel of the lower row; 68 percent of all $\rm D_m$ subhaloes have $m_{\rm acc}/M_0 > 0.05$, which puts them in the regime of short dynamical friction time scales. In terms of their orbits, $\rm D_m$ subhaloes are on orbits that are far more bound than either their $\rm D_d$ counterparts, or the 'regular' T subhaloes (left-hand panel of middle row); the median $r_{\rm c}(E)$ for $\rm D_m$ subhaloes is only 8.6 percent of the host halo's virial radius, compared to 36.5 percent and 74.3 percent for $\rm D_d$ and T subhaloes, respectively. In fact, the $r_{\rm c}(E)/r_{\rm vir}$ distribution of $\rm D_m$ subhaloes is so far offset from that of T or A subhaloes that it is clear that, on average, these subhaloes must have lost most of their orbital energy due to dynamical friction. In terms of the orbital circularity, $\eta$, $\rm D_d$ subhaloes are clearly on very radial orbits (middle panel of middle row). $\rm D_m$ subhaloes, on the other hand, have a fairly uniform distribution of orbital circularities, except for an absence of the most radial orbits. As is evident from the right-hand panel in the middle row of Fig. 15, $\rm D_d$ subhaloes typically disrupt at a halo-centric radius that is between 3 and 30 percent of the host halo's virial radius. The distribution of $r/r_{\rm vir}$ for $\rm D_m$ subhaloes is somewhat broader.

As already shown in Fig. 10, disrupting subhaloes have a bimodal distribution of $z_{\rm acc}$, with two peaks around $z_{\rm acc} \sim 0.15$ and 0.45. These correspond to subhaloes that are experiencing their first and second peri-centric passages, respectively. The lower left-hand panel of Fig. 15 reveals that the first peak is far more pronounced for $\rm D_d$ subhaloes than for $\rm D_m$ subhaloes: roughly 45 percent of $\rm D_d$ subhaloes disrupt during their first orbit (i.e., have $z_{\rm acc} \leq 0.25$). For $\rm D_m$ subhaloes this fraction is 20 percent. Finally, as evident from the lower right-hand panel of Fig. 15, a large fraction of $\rm D_m$ subhaloes (17.2 percent) have $m/m_{\rm acc} > 1$, extending all the way to $m \sim 100 m_{\rm acc}$. This is clearly not physical, but rather reflects a serious problem with the proper identification of the subhalo. As eluded to above, $\rm D_m$ subhaloes are about to merge with their host halo, which means that its phase-space distribution 'blends in' with that of its host halo. Under such conditions it is virtually impossible to determine for individual particles whether they belong to the host halo or the subhalo. Clearly, when large numbers of host-halo particles are incorrectly associated with a subhalo (and vice versa), the properties of these subhaloes can no longer be trusted. Hence, with the exception of $z_{\rm acc}$ and $m_{\rm acc}/M_0$, all distributions for the $\rm D_m$ subhaloes in Fig. 15 are unreliable and have to be taken with a serious grain of salt. The $m/m_{\rm acc}$ distribution for $\rm D_d$ subhaloes is quite different from that of its $\rm D_m$ counterparts. Only $\sim 2$ percent of $\rm D_d$ subhaloes have $m/m_{\rm acc} > 1$, and the $m/m_{\rm acc}$ distribution reveals two separate peaks; one at $m/m_{\rm acc} \sim 0.7$ and the other at $m/m_{\rm acc} \sim 0.2$; once again these correspond to subhaloes that disrupt at their first and second peri-centric passage, respectively.

One of the most intriguing findings is that disrupting subhaloes are still relatively massive. In particular, as is evident from the upper left-hand panel of Fig. 15, there are subhaloes that at the moment of their disruption still contain more than 10,000 particles. In the case of $\rm D_m$ subhaloes this is perhaps not that surprising. After all, the subhalo needs to be massive to experience sufficient dynamical friction. Recall, though, that the instantaneous masses (and hence many other properties) of $\rm D_m$ subhaloes are utterly unreliable. This is also evident from Fig. 16 which plots the evolution, during the last 0.8 Gyr prior to disruption, of various properties of ten randomly selected $\rm D_m$ subhaloes that at the moment of disruption contain more than 5,000 particles. Clearly, the majority of these evolutionary tracks are

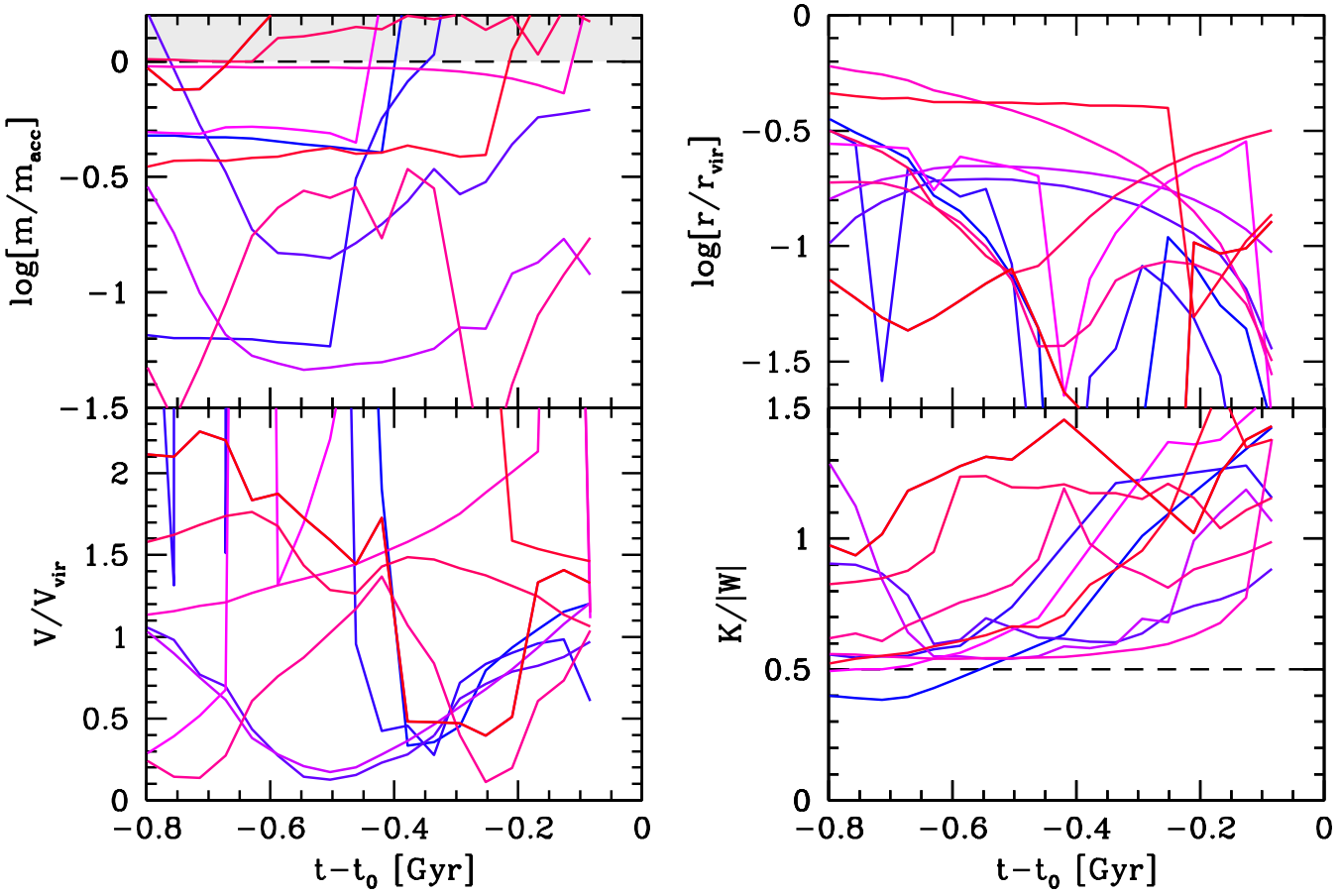


**Figure 16.** Examples of $D_m$ subhaloes in Bolshoi the last 0.8 Gyr prior to their disruption. Colored curves show the evolution of the remaining mass fraction, $m/m_{\rm acc}$ (upper left-hand panel), the host-halo-centric radius, $r/r_{\rm vir}$ (upper right-hand panel), the host-halo-centric velocity normalized by the virial velocity of the host halo, $V/V_{\rm vir}$ (lower left-hand panel), and the subhalo's virial ratio, $K/|W|$ (lower right-hand panel), for ten randomly selected $D_m$ subhaloes with more than 5000 particles at the moment of disruption. See text for detailed discussion.

fluctuating in a dramatic and unphysical way, highlighting the difficulties associated with identifying and tracking these systems.

But what are we to make of $D_d$ subhaloes that at the moment of disruption still contain thousands of particles? Idealized $N$-body simulations of individual subhaloes orbiting within an NFW host halo suggest that whenever a dark matter subhalo disrupts, it first experiences dramatic mass loss. The time between still having thousands of bound particles and complete disruption is at least an order of magnitude larger than the 42 Myr between two Bolshoi outputs. Fig. 17 shows the same as Fig. 16, but for ten randomly selected $D_d$ subhaloes with more than 5,000 particles at the moment of disruption. These evolutionary tracks are very different from those of the $D_m$ subhaloes, once more highlighting their truly distinct nature. Prior to their disruption, $D_d$ subhaloes are accelerating towards the center of their host halo, while their virial ratio is slowly increasing. All of this is perfectly consistent with $D_d$ subhaloes approaching peri-center, where they experience a tidal shock and strong tidal forces. Surprisingly, however, they do not seem to experience any significant amount of mass loss prior to their disintegration.

To summarize, there are two different 'modes' of subhalo disruption in the Bolshoi simulation (in addition to the withering described above). $D_m$ subhaloes bear all the hallmarks of merging driven by dynamical friction: they have large accretion masses (and thus short dynamical friction time scales), are on extremely bound orbits, at small halo-centric radii, and moving with low speed. As a consequence, they are difficult to identify, and most of their properties in a halo catalog cannot be trusted. The population of $D_d$ subhaloes, however, is more difficult to interpret. Their phase-space properties are consistent with them undergoing peri-centric passage along a highly-radial, deeply penetrating orbit. At peri-center the subhalo is subjected to tidal heating and to a strong tidal field, both of which are potential causes of subhalo disruption. However, neither their masses, nor their mass histories prior to disruption, are in line with expectations. Especially puzzling is the large fraction of $D_d$ subhaloes that disrupt at first peri-centric passage (see also Klimentowski et al. 2010). It remains to be seen to what extent these disruption events are physical as opposed to numerical (due to, for example, insufficient force resolution).

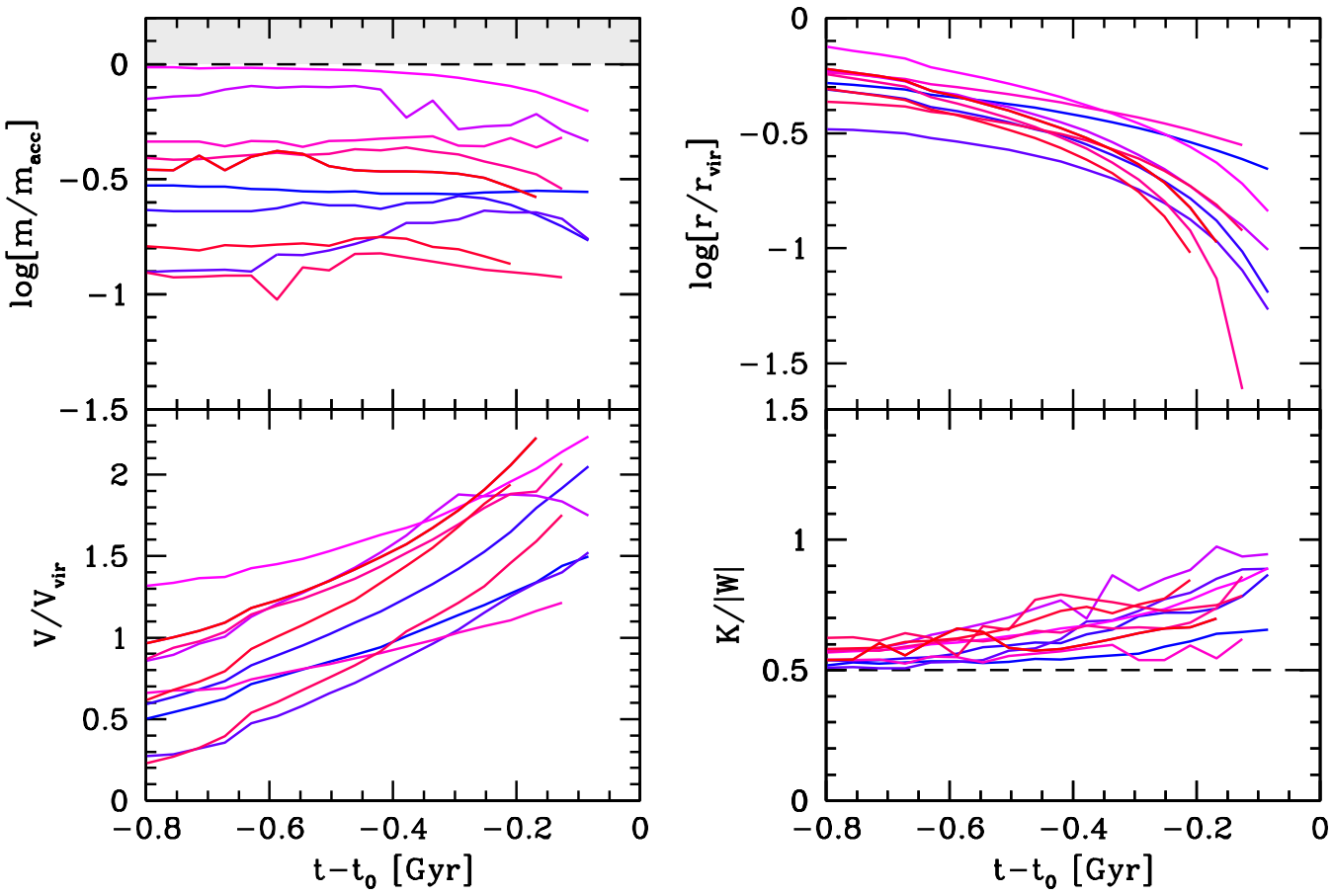


**Figure 17.** Same as Fig. 16 but for ten randomly selected $D_d$ subhaloes with more than 5000 particles at the moment of disruption.

## 6 SUMMARY

We have presented a detailed examination of the evolution of dark matter subhaloes in the cosmological Bolshoi simulation. We have identified a complete set of 12 unique subhalo evolution channels, and have analyzed the properties of subhaloes along each separate channel. The main findings are as follows:

- At the moment of accretion, subhaloes are on weakly bound orbits, with a median $r_c(E)/r_{vir}$ of 1.52 and a median orbital circularity of $\eta = 0.49$. More than eleven percent of accreting subhaloes have $r_c(E)/r_{vir} > 3$. This is very different from the distributions for all subhaloes, whose median $r_c(E)/r_{vir}$ ($\eta$) is 0.74 (0.67), and for which only 1.9 percent have $r_c(E)/r_{vir} > 3$. Hence, there is very appreciable evolution in the orbital properties of subhaloes after accretion. This is due to three effects: (i) dynamical friction, which reduces $r_c(E)/r_{vir}$ for massive subhaloes, (ii) tidal disruption, which predominantly affects subhaloes on more radial, and more bound orbits, and (iii) growth of the host halo, which causes an overall decrease of $r_c(E)/r_{vir}$ of all orbits.
- Roughly 60 percent of the present-day population of subhaloes in the Bolshoi simulation are on orbits whose apocenter falls outside of the host halo ($r_a > r_{vir}$), giving rise to a large population of ejected (or backsplash) haloes (see also Lin et al. 2003; Gill et al. 2005; Sales et al. 2007; Ludlow et al. 2009). Tidal forces cause a significant change in the orbital properties of these ejected (sub)haloes between ejection and re-accretion, mainly in the form of a loss of orbital angular momentum. As a consequence, a significant fraction of subhaloes that are ejected, and that at the moment of ejection are still bound to their host halo, are not re-accreted into the same host halo. This gives rise to 'subhalo exchange' among neighboring host haloes. We estimate that roughly $0.9 \pm 0.1$ percent of subhaloes changes their host halo per Gyr, with a weak dependence on host halo mass (see Eq. [3]). Hence, over a Hubble time, a significant fraction of all subhaloes (and thus satellite galaxies) may have changed their host halo (if they survive long enough).
- High-speed, penetrating encounters among subhaloes are very common. Hence, a significant fraction of second-order subhaloes (sub-subhaloes) in the Bolshoi halo catalog are actually first-order subhaloes undergoing an impulsive, high-speed encounter with another, more massive subhalo. We have estimated the rate of such penetrating encounters (see Eq. [14]) and find that subhaloes with a mass $m = 10^8$ $M_\odot$ orbiting inside a Milky-Way size host halo have on average about one penetrating encounter with another, more massive subhalo per dynamical time. It remains to be see what impact such penetrating, high-speed encounters have on the structure and survivability of subhaloes and their associated satellite galaxies.
- The mass and $V_{max}$ evolution of subhaloes in the Bolshoi simulation is extremely erratic, especially close to the

center of their host halo. Roughly 20 percent of Bolshoi subhaloes experience time steps in which they more than double their mass, while more than 40 (46) percent of all time steps result in an *increase* in mass ($V_{\rm max}$). Most likely these fluctuations are artifacts of the ROCKSTAR halo finder that was used to analyze the Bolshoi simulation. ROCKSTAR uses 6D phase-space information to identify subhaloes, while the Consistent merger tree algorithm uses temporal information to assure self-consistent behavior of subhaloes. Yet, we conclude that the instantaneous masses and maximum circular velocities of the resulting subhaloes are unreliable in that they undergo large, apparently random fluctuations. It remains to be seen how other subhalo finders fair in this respect.

- Half of all (first-order) subhaloes at $z = 0$ in the Bolshoi simulation were accreted onto their host haloes after $z = 0.164$. And only 1.3 (0.02) percent of all $z = 0$ subhaloes have lost more than 90 (99) percent of their mass. The absence of subhaloes with high accretion redshifts and/or with small surviving mass fractions is evidence of efficient subhalo disruption. Indeed, among the (first-order) subhaloes in the Bolshoi halo catalogs we infer a fractional disruption rate of $\sim 0.13$ Gyr$^{-1}$. By closely examining the demographics of subhaloes in the Bolshoi simulation we have identified three different 'modes' of disruption, which we refer to as 'withering', 'merging' and 'disintegration'.
- The withering mode corresponds to subhaloes that have their mass drop below the mass resolution limit (corresponding to 50 particles), and they typically continue to experience mass loss until (shortly after withering) they disappear from the halo catalogs altogether (i.e., they 'disrupt'). After correcting for the fact that a subset of these will blossom again (i.e., have their mass increase again above the resolution limit, mainly due to noise in the subhalo mass assignments), we infer a fractional withering rate of $\sim 0.10$ Gyr$^{-1}$, accounting for $\sim 77$ percent of all subhalo disruption. We emphasize that the majority of these disruption events are numerical, in that they occur below the mass resolution limit of the simulation: most of these withering subhaloes will survive (at least for an extensive period) if the simulation were to be run at higher resolution.
- The merging mode of subhalo disruption (indicated by $\rm D_m$ ) accounts for $\sim 16$ percent of all disruption events, and describes subhaloes that have lost a large fraction of their orbital energy due to dynamical friction. At the moment of disruption they are on extremely bound orbits, at small halo-centric radii, and moving with low speed. They 'merge' with the background of the host halo, simply because they can no longer be identified as a self-bound entity, even in 6D phase-space. As a consequence, most of their properties in a halo catalog (shortly before disruption) cannot be trusted. Subhaloes that disrupt along this channel are typically very massive with more than 68 percent having a mass at accretion that is larger than 5 percent of the present day host mass.
- The disintegration mode of subhalo disruption, indicated by $\rm D_d$ , accounts for the final 7 percent of all subhalo disruption events. Unlike $\rm D_m$ subhaloes, there is no indication that $\rm D_d$ subhaloes have experienced appreciable dynamical friction. Their phase-space properties, at the moment of disruption, are consistent with them undergoing peri-centric passage along a highly-radial, deeply penetrating orbit. At peri-center the subhalo is subjected to tidal heating and a strong tidal field, both of which may potentially cause subhalo disruption. However, neither their masses, nor their mass histories prior to disruption, are in line with expectations. In particular, the mass function of $\rm D_d$ subhaloes, at the moment of disruption, is indistinguishable from that of all subhaloes, and they experience little to no mass loss in the 0.8 Gyr leading up to their disruption. These aspects are difficult to reconcile with physical disruption due to tidal heating and/or stripping, and we suspect that these disruption events are also numerical (most likely due to inadequate force resolution). If correct, this bring the fractional numerical disruption rate of subhaloes in the Bolshoi simulation to 0.11 Gyr$^{-1}$, compared to a fractional rate of true (physical) disruption of 0.02 Gyr$^{-1}$.

We conclude that present-day cosmological simulations are still subject to significant numerical over-merging. Depending on whether the 'disintegration mode' is numerical or physical, we infer that between 77 and 84 percent of all subhalo disruption in the Bolshoi simulation, as inferred from the publicly available ROCKSTAR halo catalogs, is numerical. And this is an underestimate of the actual artificial disruption; recall that the Consistent merger tree algorithm of Behroozi et al. (2013b) already attempted to correct the halo catalogs for artificial disruption, by removing all subhaloes, and all their progenitors, that at the moment of disruption do not experience a tidal acceleration exceeding the limit of $|\mathcal{T}| = 0.4\,{\rm km\,s^{-1}\,Myr^{-1}}$ comoving ${\rm Mpc}^{-1}$ (see §2.2). Since these systems are no longer present in the halo catalogs, they are not included in our analysis. Consequently, the fractional disruption rates discussed above are to be considered lower limits. We also point out that the tidal limit of $0.4\,{\rm km\,s^{-1}\,Myr^{-1}}$ comoving ${\rm Mpc}^{-1}$ is fairly arbitrary, and it therefore should not come as a surprise that a significant fraction of the remaining disruption events are numerical as well.

The presence of significant amounts of artificial subhalo disruption in numerical simulations has important implications. It is a serious road-block in any attempt to use numerical simulations to interpret clustering on small scales. In principle this may be circumvented by allowing for 'orphan' galaxies (i.e., galaxies without associated subhaloes), something that is commonly done in semi-analytical models for galaxy formation (e.g., Wang et al. 2006; Kitzbichler & White 2008; Guo et al. 2011), but such a treatment is crude at best. In addition, over-merging in simulations is also a serious concern for (hydro)-simulations of galaxy formation, especially if they are used to predict properties of satellite galaxies and/or stellar haloes (intra-cluster light). In a forthcoming paper (van den Bosch et al. 2016, in prep.), we use a large suite of idealized numerical simulations to examine the conditions under which subhaloes in $N$-body simulations experience numerical and/or physical disruption, in an attempt to shed some light on this important, outstanding issue.

## ACKNOWLEDGMENTS

I am indebted to Peter Behroozi for all his help with the halo catalogs of the Bolshoi simulation, and to Fangzhou Jiang, Andrew Hearin and Duncan Campbell for valuable

discussion. FvdB is supported by the Klaus Tschira Foundation and by the US National Science Foundation through grant AST 1516962. Part of this work was performed at the Aspen Center for Physics, which is supported by National Science Foundation grant PHY-1066293.

## REFERENCES

Amara A., Metcalf R.B., Cox T.J., Ostriker J.P., 2006, MNRAS, 367, 1367
Behroozi P.S., Wechsler R.H., Wu H.-Y., 2013a, ApJ, 762, 31
Behroozi P. S., Wechsler R. H., Wu H.-Y., Busha M.T., Klypin A.A., Primack J.R., 2013b, ApJ, 763, 18
Binney J., Tremaine S., 2008, Galactic Dynamics, Princeton University Press
Bradač M., Schneider P., Steinmetz M., Lombardi M., King L. J., Porcas R., 2002, A&A, 388, 373
Bradač M., Schneider P., Lombardi M., Steinmetz M., Koopmans L.V.E., Navarro J.F., 2004, A&A, 423, 797
Brainerd, T. G., Goldberg, D. M., & Villumsen, J. V. 1998, ApJ, 502, 505
Bryan G., Norman M., 1998, ApJ, 495, 80
Carlberg R. G., 2009, ApJ, 705L, 223
Conroy C., Wechsler R. H., Kravtsov A. V., 2006, ApJ, 647, 201
Conroy C., Wechsler R. H., Kravtsov A. V., 2007, ApJ, 668, 826
Croton D.J., et al., 2006, MNRAS, 365, 11
Dalal N., Kochanek C. S., 2002, ApJ, 572, 25
Dekel A. et al., 2009, Nature, 457, 451
De Lucia G., Blaizot J., 2007, MNRAS, 375, 2
Diemand J., Moore B., Stadel J., 2004, MNRAS, 352, 535
Diemand J., Kuhlen M., Madau P., 2007, ApJ, 667, 859
Eddington A.S., 1913, MNRAS, 73, 359
Fakhouri O., Ma C.-P., Boylan-Kolchin M., 2010, MNRAS, 406, 2267
Fontanot F., Springel V., Angulo R.E., Henriques B., 2012, MNRAS, 426, 2335
Gao L., White S. D. M., Jenkins A., Stoehr F., Springel V., 2004, MNRAS, 355, 819
Ghigna S., Moore B., Governato F., Lake G., Quinn T., Stadel J., 1998, MNRAS, 300, 146
Ghigna S., Moore B., Governato F., Lake G., Quinn T., Stadel J., 2000, ApJ, 544, 616
Gill S.P.D., Knebe A., Gibson B.K., 2005, MNRAS, 356, 1327
Giocoli C., Pieri L., Tormen G., 2008, MNRAS, 387, 689
Giocoli C., Tormen G., Sheth R.K., van den Bosch F.C., 2010, MNRAS, 404, 502
Guo Q., et al., 2011, MNRAS, 413, 101
Hayashi E., Navarro J.F., Taylor J.E., Stadel J., Quinn T., 2003, ApJ, 584, 541
Han J., Jing Y.P., Wang H., Wang W., 2012, MNRAS, 427, 2437
Hearin A. P., Zentner A. R., Berlind A. A., Newman J. A., 2013, MNRAS, 433, 659
Hearin A.P., Watson D.F., Becker M.R., Reyes R., Berlind A.A., Zentner A.R., 2014, MNRAS, 444, 729
Hearin A.P., Zentner A.R., van den Bosch F.C., Campbell D., Tollerud E., 2016, MNRAS, 460, 2552
Ibata R. A., Lewis G. F., Irwin M. J., Quinn T., 2002, MNRAS, 332, 915
Jiang F., van den Bosch F.C., 2016a, MNRAS, 458, 2848
Jiang F., van den Bosch F.C., 2016b, MNRAS, submitted (arXiv:1610.02399)
Jiang L., Cole S., Sawala T., Frenk C.S., 2015, MNRAS, 448, 1674
Kang X., van den Bosch F.C., 2008, ApJ, 676, 101
Kauffmann G., Nusser A., Steinmetz M., 1997, MNRAS, 286, 795
Keeton C. R., Moustakas L. A., 2009, ApJ, 699, 1720
Kitzbichler M.G., White S.D.M., 2008, MNRAS, 391, 1489
Klimentowski J., Lokas E.L., Knebe A., Gottlöber S., Martinez-Vaquero L.A., Yepes G., Hoffman Y., 2010, MNRAS, 402, 1899
Klypin A., Gottlöber S., Kravtsov A.V., Khokhlov A.M., 1999, ApJ, 516, 530
Klypin A.A., Trujillo-Gomez S., Primack J.R., 2011, ApJ, 740, 102
Knebe A., Knollmann S.R., Muldrew S.I., Pearce F.R., Aragon-Calvo M.A., Ascasibar Y., Behroozi P.S., Ceverino D., 2011, MNRAS, 415, 2293
Knebe A., Pearce F. R., Lux H., Ascasibar Y., Behroozi P. S., Casado J., Moran C. C., Diemand J., 2013, MNRAS, 435, 1618
Knollmann S.R., Knebe A., 2009, ApJS, 182, 608
Kravtsov A.V., Klypin A.A., Khokhlov A.M., 1997, ApJS, 111, 73
Lehmann B.V., Mao Y.-Y., Becker M.R., Skillman S.W., Wechsler R.H., 2015, preprint (arXiv:1510.05651)
Lin W.P., Jing Y.P., Lin L., 2003, MNRAS, 344, 1327
Ludlow A.D., Navarro J.F., Springel V., Jenkins A., Frenk C.S., Helmi A., 2009, ApJ, 692, 931
Maciejewski M., Colombi S., Springel V., Alard C., Bouchet F.R., 2009, MNRAS, 396, 1329
Maccìo A.V., Moore B., Stadel J., Diemand J., 2006, MNRAS, 366, 1529
Marín F.A., Wechsler R.H., Frieman J.A., Nichol R.C., 2008, ApJ, 672, 849
Metcalf R. B., Madau P., 2001, ApJ, 563, 9
Moore B,. Katz N., Lake G., 1996, ApJ, 457, 455
Moore, B., Governato, F., Quinn, T., Stadel, J., & Lake, G. 1998, ApJ , 499, 5
Muldrew S.I., Pearce F.R., Power C., 2011, MNRAS, 410, 2617
Navarro J.F., Frenk C.S., White S.D.M., 1997, ApJ, 490, 493
Neistein E., Dekel A., 2008, MNRAS, 383, 615
Peñarrubia J., Benson A.J., Walker M.G., Gilmore G., McConnachie A.W., Mayer L., 2010, MNRAS, 406, 1290
Pieri L., Bertone G., Branchini E., 2008, MNRAS, 384, 1627
Reddick R.M., Wechsler R.H., Tinker J.L., Behroozi P.S., 2013, ApJ, 771, 30
Reddick R.M., Tinker J.L., Wechsler R.H., Lu Y., 2014, ApJ, 783, 118
Sales L.V., Navarro J.F., Abadi M.G., Steinmetz, M., 2007, MNRAS, 379, 1475
Springel V. et al., 2008, MNRAS, 391, 1685
Taffoni G., Mayer L., Colpi M., Governato F., 2003, MNRAS, 341, 434
Taylor J. E., Babul A., 2001, ApJ, 559, 716
Taylor J. E., Babul A., 2004, MNRAS, 348, 811
Tormen G., 1997, MNRAS, 290, 411
Tormen G., Bouchet F.R., White S.D.M., 1997, MNRAS, 286, 865
Tormen G., Diaferio A., Syer, D., 1998, MNRAS, 299, 728
Tóth G., Ostriker J. P., 1992, ApJ, 389, 5
Vale A., Ostriker J. P., 2004, MNRAS, 353, 189
van den Bosch F.C., Lewis G.F., Lake G., Stadel J., 1999, ApJ, 515, 50
van den Bosch F.C., Tormen G., Giocoli C., 2005, MNRAS, 359, 1029
van den Bosch F.C., Jiang F., 2016, MNRAS, 458, 2870
van den Bosch F.C., Jiang F., Hearin A., Campbell D., Watson D., Padmanabhan N., 2014, MNRAS, 445, 1713
van den Bosch F.C., Jiang F., Campbell D., Behroozi P., 2016, MNRAS, 455, 158
Wang L., Li C., Kauffmann G., De Lucia G., 2006, MNRAS, 371, 537
Wetzel A.R., 2011, MNRAS, 412, 49
Xu D.D., Sluse D., Gao L., Wang J., Frenk C.S., Mao S., Schneider P., Springel V., 2015, MNRAS, 447, 3189

Zentner A.R., Bullock J.S., 2003, ApJ, 598, 49
Zentner A. R., Berlind A. A., Bullock J. S., Kravtsov A. V., Wechsler R. H., 2005, ApJ, 624, 505
Zentner A.R., Hearin A., van den Bosch F.C., 2014, MNRAS, 443, 3044
Zentner A.R., Hearin A., van den Bosch F.C., Lange J.U., Villarreal A., 2016, preprint (arXiv:1606.07817)

## APPENDIX A: IMPACT OF MASS ERROR ON SUBHALO MASS FUNCTION

As shown in §5.1, the mass and $V_{\rm max}$ histories of individual subhaloes are extremely 'noisy', revealing an erratic behavior in which subhaloes occasionally undergo large, and unexpected,*increases* in either mass or maximum circular velocity. These most likely reflect errors in the ROCKSTAR halo finder. We now investigate how these errors in the instantaneous subhalo masses impact the ability to measure a reliable subhalo mass function.

Let $P(Q){\rm d}Q$ be the distribution of $Q \equiv \log[m(t+\Delta t)/m(t)]$ shown in the left-hand panel of Fig. 13. If we interpret time steps in which the subhalo gains mass (i.e., for which $Q>0$) as entirely due to errors in the assigned subhalo mass, then we may interpret the symmetric version

$$P_{\rm sym}(Q) = \begin{cases} P(Q) & \text{if } Q \geq 0 \\ P(-Q) & \text{if } Q < 0 \end{cases} \qquad \text{(A1)}$$

as a measure of the distribution of the instantaneous errors in subhalo mass. In doing so, we interpret $Q$ as equal to $\log[1+\Delta m/m]$, with $\Delta m$ the instantaneous mass error. We can use this to estimate the impact on the subhalo mass function, by convolving a 'true' subhalo mass function, $n_0(m) \equiv {\rm d}N/{\rm d}(m/M_0)$, where $M_0$ is the mass of the host halo, with this 'error kernel function', according to

$$n_{\rm conv}(m) = \int n_0(10^Q\, m)\, P(Q)\, {\rm d}Q\,. \qquad \text{(A2)}$$

As an example, we adopt the universal functional form of the (evolved) subhalo mass function advocated in Jiang & van den Bosch (2016) as representative of a typical $n_{\rm true}(m)$, and use Eqs. (A2) and (A1) to compute $n_{\rm conv}(m)$. The results are shown in Fig. A1, where the red and blue curves correspond to $n_0(m)$ and $n_{\rm conv}(m)$, respectively. Clearly, the errors on $m$, as represented by $P_{\rm sym}(Q)$, have a completely negligible impact on the subhalo mass function, except for the exponential tail at the massive end, where Eddington bias (Eddington 1913) causes a systematic overestimate of the abundance of massive subhaloes. Since that end of the mass function is anyways uncertain due to limiting statistics (i.e., the Poisson errors are huge), we can safely conclude that although individual subhaloes can carry substantial errors on their instantaneous masses, these errors have no significant impact on the subhalo mass function. By analogy, the same applies for the subhalo $V_{\rm max}$ function.

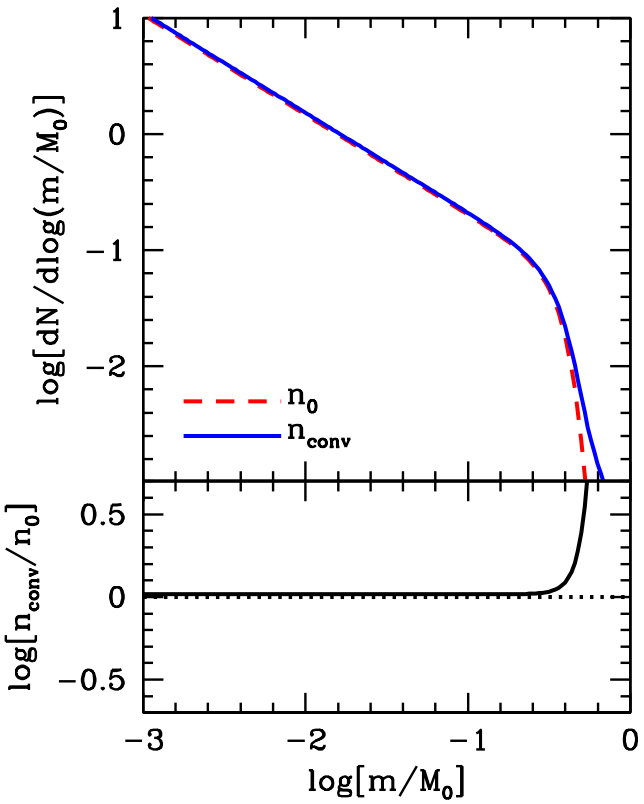


**Figure A1.** Impact of errors on instantaneous subhalo mass on the subhalo mass function. The red, dashed curve in the upper panel is a typical subhalo mass function, $n_0 = {\rm d}N/{\rm d}(m/M_0$, described in the text. The blue, solid curve is the subhalo mass function one obtains after convolving $n_0(m)$ with the error kernel function $P(Q)$, which describes the probability that an instantaneous halo mass carries an error $\Delta m = m\,[10^Q - 1]$. The lower panel plots the logarithm of the ratio $n_{\rm conv}/n(m)$. As is evident, the convolved subhalo mass function is indistinguishble from the original one, except at the very massive end (Eddington bias).